NATIONAL TECHNICAL UNIVERSITY OF ATHENS
SCHOOL OF NAVAL ARCITECTURE AND MARINE ENGINEERING
SHIPBUILDING TECHOLOGY LABORATORY

MEASUREMENT OF RESIDUAL STRESSES IN COMPOSITE MATERIALS WITH THE INCREMENTAL HOLE DRILLING METHOD

Diploma Thesis

by
Konstantinos Stamatopoulos

Advisor:
Assoc. Professor Nicholas Tsouvalis

June 2011
Athens

AKNOWLEDGEMENTS

For their gracious support and their vital help in the completion of this study I would like to express thanks to:

The Shipbuilding Technology Laboratory staff, especially Mr Athanasios Markoulis and Mr Charis Xanthis, for their contribution in the execution of the experimental tests program of this study,

Mr Georgios Margelis, PhD student of the School of Naval Architecture and Marine Engineering, for his contribution in the experimental tests program and his valuable advice and guidance in all the aspects of this study,

Finally, my supervising professor, Mr Nicholas Tsouvalis, Associate Professor of the School of Naval Architecture and Marine Engineering, for his guidance and advice throughout the project, for his patience until its completion, and the experience I gained from this collaboration.

CONTENTS

1. INTRODUCTION

1.1 General

Residual stresses are generally called the stresses that develop in a material without the application of external loads. They can be found in most composite laminates. Residual stresses can develop either during manufacturing or operation of the composite structure. Since they can have a large magnitude they may affect the strength of composite structures and their external load bearing capacity [1].

They usually develop because of mechanical properties mismatch between the matrix and the reinforcing fibres. Residual stresses can appear in three different length scales: fibre-matrix, lamina-laminate and structural scale. One of the mechanisms creating residual stresses is the differential thermal expansion due to difference of the thermal expansion coefficients between the fibres and the matrix and also between the plies having different directions. Tool-part interaction is another basic mechanism that occurs when a laminate with a low Coefficient of Thermal Expansion (CTE) is cured on a tool with a much higher CTE. Cure shrinkage is another basic mechanism which creates residual stresses. It is a chemical effect that takes place during curing when the polymer volume decreases and leads to a high level of locked in stresses [1].

There are various methods to estimate the residual stresses in a composite structure. In this work the method used is the incremental hole drilling method. Various specimens were constructed out of different materials commonly used in shipbuilding. Then, using the incremental hole drilling method residual stresses were measured in different parts of each specimen.

2. RESIDUAL STRESSES IN COMPOSITE MATERIALS: A SHORT REVIEW

2.1 Basic mechanisms creating residual stresses

Residual stresses in composite materials can build up on three different length scales: fibre-matrix, lamina-laminate and structural scale. These three levels of stresses are also called intralaminar, interlaminar and laminate stresses, respectively. The sources of residual stresses can be classified as intrinsic (related to material, lay-up and structure shape) or extrinsic (related to processing and tooling). The main effects of residual stresses are reduction in strength, and shape distortion. Stresses at the fibre-matrix, lamina-laminate and structural levels all affect the strength of the component, whereas only lamina-laminate and structural level stresses affect dimensional stability to any significant degree. Figure 2.1 shows a schematic of the relationship between the source of stress, the length scale at which it is acting, and the effect of that stress [2].

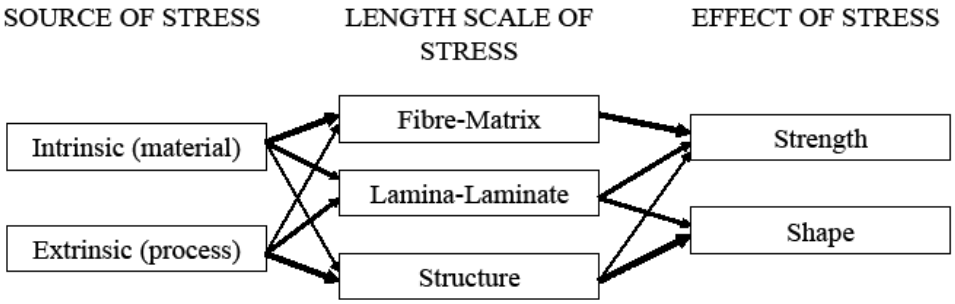

Figure 2.1: Schematic of the relationship between stress source, length scale of stress, and the effect of residual stress. Thicker arrows indicate a stronger relationship (Figure from reference [2]).

Differential thermal expansion is one of the basic mechanisms creating residual stresses whose effects can be observed in all three of the above mentioned levels of residual stresses. At the micro-mechanical level (intralaminar), the difference between the thermal expansion coefficient of the fibres and the matrix is the main cause for the development of residual stresses. The cooling during the curing cycle causes a volumetric shrinkage of the matrix, which is significantly higher than the fibre shrinkage. A second level of stresses in continuous-fibre-reinforced composites is the level which forms on the ply-to-ply scale (interlaminar) in multiaxial laminates due to the different CTEs of the individual plies in different directions. These are referred as 'macro-stresses' (macro-mechanical or lamination residual stresses according to reference [3]) and they are present on a ply-to-ply scale due to lamina anisotropy [4]. In the laminate level, residual stresses occur through the thickness and are typically parabolic in distribution. Such stresses in uniaxial laminates can be of the order of 40 MPa and affect the mechanical response of the composite. Also, such stresses can cause dimensional tolerance problems in asymmetrically cooled laminates. One important point concerning the stresses that occur at this level is that they can be eliminated by raising the composite above the glass transition temperature (T_g) of the matrix, and allowing relaxation processes to occur [4].

Tool-part interaction occurs when a low CTE laminate is cured on a tool with a considerably higher CTE. Aluminium or steel tools have much higher CTEs than composite parts, and tend to stretch the parts as they heat up. This can happen as a result of small shear stresses at the tool interface causing tension in the structure. In plane stresses can

arise through the thickness in different levels and as a result cause bending when the stresses are released [1].

Other mechanisms may create residual stresses on composites such as cure shrinkage, moisture, aging, elevated temperature post-cure, material properties fluctuation on the microscopic scale, free surface, differences in fibre-volume fraction and non-uniform degree of cure [1].

In order to estimate the actual stress state present when a structure is subjected to external loading, the residual stress state must be superimposed on any stress state resulting from external loading. When the total stress exceeds the design stress limit of the material, this type of combined stress can result in premature structural failure. Therefore, the evaluation of residual stresses is an important factor in predicting the failure mode of a composite [5, 6].

On the structural scale a tertiary level of stresses exists due to differential thermal histories of structures of a laminate during the cooling process. Such stresses are called global stresses and occur through the thickness of a laminate and are typically parabolic in distribution. In general, a thick laminate will experience a slower cooling rate in the centre of the laminate than at the surface plies. At a certain temperature, the centre plies may still need to solidify, whereas the surface plies may have already become solid. Upon further cooling, the surface plies impose a constraint on the shrinkage of the centre plies. This will often result in the parabolic distribution of compressive residual stresses in the surface plies and tensile stresses in the centre plies [2].

Figure 2.2a shows a typical cure cycle for a thermoset composite, where the approximate material behavior is indicated in italics. Figure 2.2b shows the typical relaxation behavior of resin after gelation. Before gelation the matrix is viscous and no residual stresses can be carried by the matrix. After gelation, the matrix is a rubbery viscoelastic solid with very short relaxation times. At the end of the final temperature hold, the matrix is fully cured and behaves as a viscoelastic glassy solid with a very long relaxation time. The majority of the residual stresses are generated during the cooling down from the final hold temperature. These stresses are the easiest to predict as the material can be treated as being thermoelastic with fairly good accuracy. Stresses built up earlier in the cure cycle, for example due to cure shrinkage and tool-part interaction, are more difficult to estimate [2].

According to reference [7], during curing of thermoset composites, the resin undergoes cross-linking reactions that lead to an increase of material density and reduction in volume.

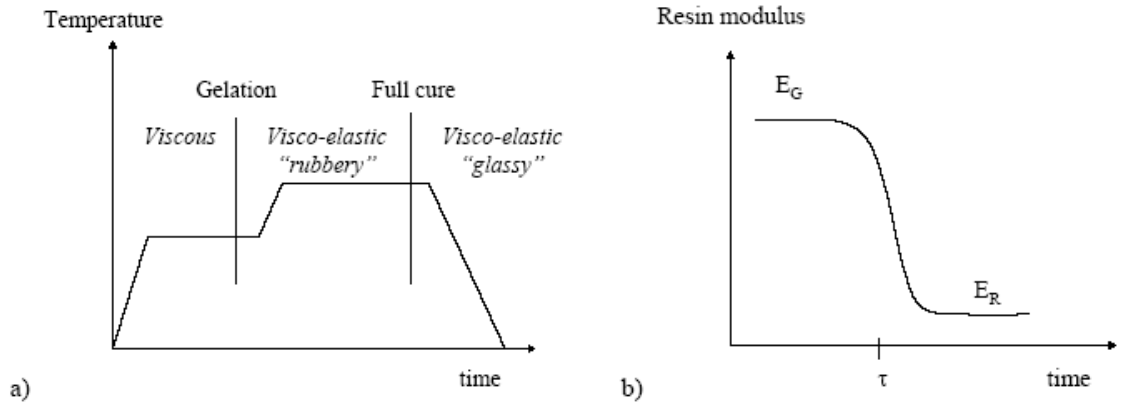

Figure 2.2: a. Schematic of a typical cure cycle showing the material behavior at different times.
b. Schematic of relaxation behavior of resin after gelation (Figure from reference [2]).

The curing process starts with the resin as a monomer, then moves on to linear growth and branching, forms a gelled but incompletely cross linked network and ends with an infinite cross-linked network when the resin has cured. The process of volume reduction, usually referred as chemical shrinkage, together with thermal contractions can lead to development of high locked-in stresses when there is constraint. These thermal and resin shrinkage induced stresses can subsequently cause distortion and premature cracking of the

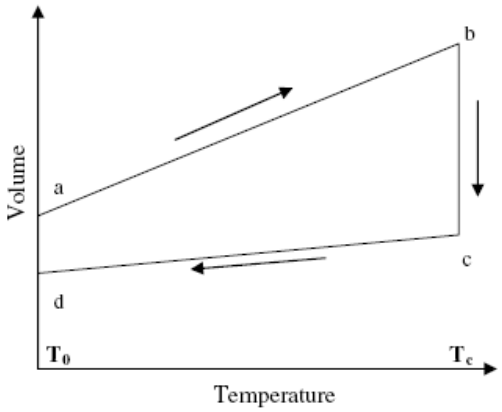

Figure 2.3: Schematic of volume change of epoxy resin during cure (Figure from reference [7]).

composite moulding [7].

Moreover, according to the same reference [7], an idealized schematic of the volumetric change of epoxy due to thermal expansion and chemical contraction is shown in Figure 2.3. The stages from a to d are described as follows:

Stage a-b: the volume of the resin increases when it is instantaneously heated up from reference temperature T_o to the curing temperature, T_c, due to thermal expansion before any chemical shrinkage occurs.

Stage b-c: the volume decreases due to chemical shrinkage at a constant temperature and the resin vitrifies.

Stage c-d: the volume decreases due to thermal contraction when it cools down to room temperature. The slope of the line c-d is lower than the slope of line a-b, because the coefficient of thermal expansion in the glassy state is lower than in the rubbery state [7].

The match of the results from three different cure cycles suggested that cure shrinkage is only a function of the degree of cure, regardless of time and temperature [7].

The above-mentioned changes of volume during curing were taken into consideration during the design phase of the current experimental tests program as described in the following paragraph 4.3.

If residual stresses are not taken into account during the structural design phase, then a higher safety factor should be considered for the structure, often leading to over-weight and over-designed structures.

2.2 Influence of the development of residual stresses in composite materials

Residual stresses in composite structures can cause defects such as fibre waviness, cracking, delamination, warpage, dimensional instability and spring-in.

The fibre waviness in unidirectional materials develops when the fibres deviate from the mean direction of the laminate, forming a pattern that can usually be mathematically represented by a sine wave (Figure 2.4). Fibre waviness develops during the manufacturing of a composite structure when the fibres are subjected to compressive axial loads from thermal residual stresses. Since the matrix cannot provide any transverse support, the fibres are deformed (micro-buckling) and waviness is developed. Fibre waviness reduces the strength of the structure as well as the overall quality of the composite material [8].

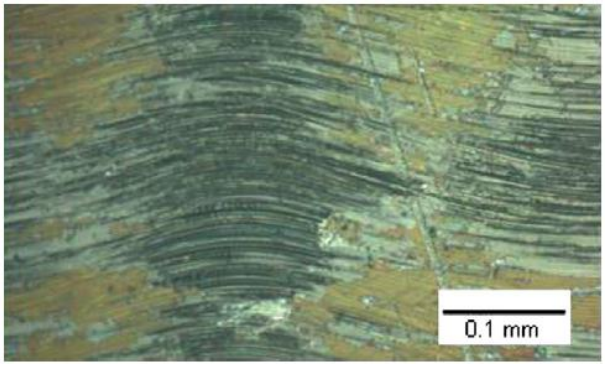

Figure 2.4: Micrograph of a composite laminate showing fibre waviness (Figure from reference [8]).

According to reference [8], thermal residual stresses may cause cracking in composite materials, when they exceed the yield strength of the resin. When the fibre-matrix interface bond is weak, cracks can propagate along the interface. When a strong interface is present, cracks may propagate into the matrix. The thermal residual stresses can reach values of the same order as the transverse ply strength, which may cause the ply to crack prematurely during processing. The above-mentioned cracks, usually referred to as microcracks, can sometimes be visible in transparent composites and provide failure initiation sites in subsequent service life. Microcracks may grow into transverse ply cracks, which form initiation points for delamination and eventually failure of the laminate, such as longitudinal splitting. More importantly, they can cause premature failure in cyclic loading conditions [8].

Apart from the creation of transverse cracks, the difference of the magnitude of residual stresses between 0° and 90° plies in cross-ply laminates can also lead to delamination. Interlaminar failure of composite materials is characterized by gradual propagation of the delamination which finally leads to loss of stiffness and strength of the structure. Another mechanism causing delamination is the free edge effect, which also leads to matrix cracking. Delamination at free edges is associated with high interlaminar stresses, which are developed due to the discontinuity of properties at the free edges. Delamination may also occur around any geometric stress concentration, for example around holes, cut-outs and generally changes in section, and this reduces considerably the capability of the composite structure to bear loads [8].

The ability to fabricate composite structures within tight dimensional tolerances is a very important factor for affordable composite manufacturing. Residual stresses arise during the processing of composite structures and they often result in dimensional changes, warpage of structures fabricated on flat tooling, as well as spring-in of flanges on angled sections [4]. These kinds of defects can more easily be observed in thin laminates where the magnitude of the deformation is usually larger, especially in the case of warpage. Warpage or

dimensional instability may be the result of two mechanisms: unbalanced cooling and tool-part interaction. The tool-part interaction has been found to contribute significantly to warpage, especially for thin pieces. Moreover, a non-uniform temperature distribution in the

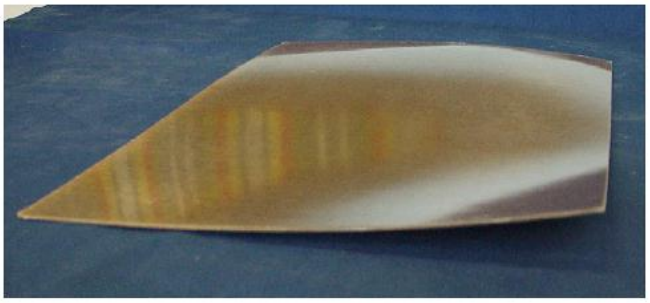

Figure 2.5: Distorted glass fibre fabric reinforced polyetherimide laminate (Cetex®) due to non-uniform cooling of the hot platen press (Figure from reference [8]).

mould may cause warpage, as can be seen in Figure 2.5 [8].

2.3 Objectives

In the experiments performed for this study the residual strains were measured through the thickness of the specimen by the use of the incremental hole-drilling method in materials commonly used in the shipbuilding industry. The objective was to assess the level of the residual stresses in this kind of materials. Furthermore, by measuring the strains in different parts of the specimens it was examined whether or not the tool-imposed restrictions to the shrinkage or expansion of the composite affected the magnitude of the residual stresses.

3. EXPERIMENTAL METHODS FOR THE ESTIMATION OF RESIDUAL STRESSES IN COMPOSITE MATERIALS

The experimental methods for the estimation of residual stresses are divided in general into two categories: destructive and non-destructive. Furthermore, the non-destructive methods are divided into those that use the inherent material properties, the ones that use sensors and finally those that use in-plane and out of plane deformation. The non-destructive methods in general can provide results for a fairly large part of a laminate whereas the measurements acquired using destructive methods concern only a small area of the structure.

3.1 Methods utilizing the inherent material properties of the composites

Some material properties of the composites change when the material is exposed to stresses or stains. In this chapter the techniques that can measure this change of properties are presented.

3.1.1 Photo-elasticity

Photo-elasticity is a classical optical technique for static stress analysis. For the determination of the stress field in composite materials using this method, a transparent or translucent matrix is required. When stress is applied in such materials, the molecular orientation distribution changes, which affects the polarisation state of the light (photo-elasticity). For determination of the magnitude of residual stresses, measurement of retardation (phase difference between two light vectors travelling at different velocities) is required, from which the residual stress components can be calculated by means of the stress-optic law (or ‘‘Brewster’s law’’). Photo-elasticity can be used to determine the thermal residual stress distribution in the matrix, when a unidirectional specimen with fibres in the 0° direction is rotated between crossed polarisers with respect to the polarisers. The matrix region then forms a fringe indicating a unique principal stress direction. Maximum extinctions are found at 0° and 90°, which indicates that the principal stress directions are parallel and perpendicular to the fibre direction [3].

A drawback of this method is that it can only be used in thin composites with low fibre volume fraction (i.e. <40 Vol%) in order to be able to observe any effects in the matrix. The residual stress patterns in both matrix and reinforcing phase in the cross-section of unidirectional composites with regular (high) fibre volume fraction can be observed if a thin slice of the cross-section is cut and then held between crossed polarisers in transmitted polarised light [3].

3.1.2 Micro-Raman spectroscopy

Micro-Raman Spectroscopy (MRS) is another experimental method for the determination of residual strains, based on an intrinsic material property. This method is based on the stress (strain) sensitivity of most Raman vibrational modes of crystalline phases. The difference in energy between the incident photon and the Raman scattered photon is equal to the energy of a vibration of the scattering molecule. A plot of intensity of scattered light

versus energy difference is a Raman spectrum. Raman spectroscopy can be used for the determination of strain in carbon fibres embedded in a translucent polymer matrix, since some peaks in the Raman spectrum of the fibre, will change when strain is applied. For example, the Raman peaks of the fibre in an unloaded Polyetheretherketone (PEEK) prepreg show a shift to higher peak positions. This represents a compressive fibre strain due to thermal residual strains imposed by the surrounding matrix. In Figure 3.1, the shift of the 2660 cm^{-1} peak with compressive strain (-0.65% versus 0%) is shown. At first, a calibration curve on single fibres in air should be established, in order to relate the change in the Raman

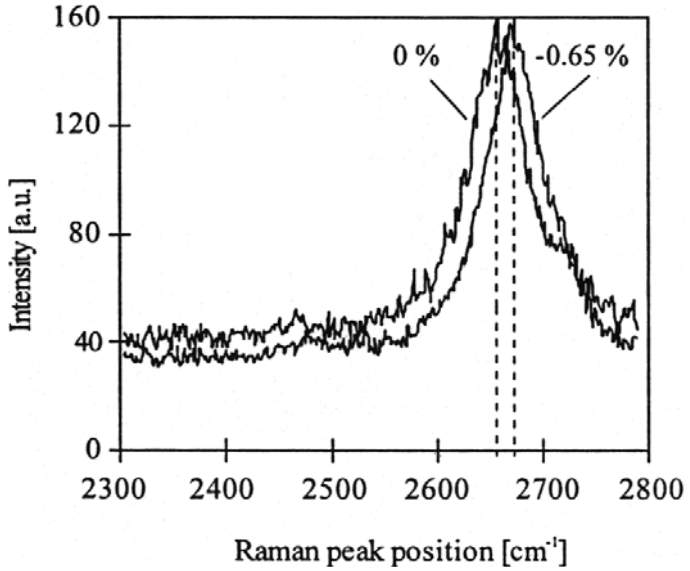

Figure 3.1: Raman spectrum which presents the shift of the 2660 cm^{-1} peak for AS4 carbon fibres embedded in PEEK matrix (Figure from reference [3]).

peak position to the magnitude of fibre thermal residual strain within the composite. This method applies to unidirectional composite prepreg layers (PEEK) with fibre volume fractions of 60% or higher, or composites with more unidirectional plies. Certain amorphous fibres, such as glass, have a very weak Raman response and they cannot be used as strain sensors. In order to solve this problem, a small amount of aramid fibres can be placed in glass fibre reinforced composites, since they exhibit very strong Raman responses. The Raman spectroscopy method can also be used for the determination of interply stresses in cross-ply laminates (macro-mechanical stresses), by positioning of aramid fibres in glass reinforced laminates. With the MRS method, the residual strains can be measured in small steps down to 1-2 με. Also, there is no need for analytical models to predict the macroscopic residual stresses. However, the contribution of the matrix to the Raman peaks should be taken into consideration, otherwise there would be an over-estimation of the magnitude of the residual stresses [1], [3].

3.1.3 Measurement of electrical conductivity of fibres

Another method involves the measurement of the electrical resistance of the materials. This method requires an electrically conductive material, so a polymer which is insulating is not suitable. However, polymers containing electrically conductive fillers are suitable and so are composites reinforced with continuous carbon fibres since carbon fibres are electrically conductive [9].

The electrical properties of carbon fibre composite materials, such as the electric resistance, are affected by strain, damage and temperature. Monitoring the electric resistance of a composite material provides information for the stresses and the temperature, without the need for embedding sensors which increase the cost and may reduce the strength of the structure. This leads to the possibility of determining differences in the interlaminar residual stresses by means of electrical resistivity measurements. In order to estimate the magnitude of the residual stresses by using this method, further development of this technique is necessary, since residual stresses cannot yet be calculated accurately [3].

According to reference [9], the effect of a structural transition of the matrix (i.e. glass transition, melting, solid-state curing), on the fibre morphology (e.g. fibre waviness), results in an increase in the electrical resistivity of the composite in the fibre direction. The thermal stress leads to an increase in the degree of fibre waviness or a decrease in the degree of fibre alignment. Therefore, the measurement of electrical conductivity of the fibres may reveal information concerning the residual stresses, structural transitions, thermal damage, etc [9].

3.2 Measurement methods using sensors

Methods that use sensors are capable of measuring change in the residual strains of a composite through change of its properties, providing that there is appropriate mechanical interaction between the composite and these sensors. Such kinds of sensors are strain gauges and optic sensors which are used for the studying of interlaminar stresses in angle-ply laminates as well as intralaminar stresses in unidirectional laminates [3].

3.2.1 Embedded strain gauges

Embedded strain gauges in thermoset composites have been shown to give accurate results during heating as well as cooling but they cannot be used in thermoplastic composites because of the high processing temperatures [1]. In one case it was reported that in unidirectional Carbon Fibre/PEEK (CF/PEEK) laminates, a strain gauge was melt-embedded in the centre of the surface plies for a short melt time, in order to directly measure residual strain development from both thermal and crystallisation effects [3].

3.2.2 Embedded fibre optical sensors

Fibre Optical Sensors (FOSs) can be embedded inside a composite material, where they act as sensors which monitor the residual strains. These sensors are small in size and lightweight and as such, they can be embedded in a composite laminate without significantly compromising its structural integrity [10]. Applications of the Fibre Optical Sensors are found in both unidirectional and angle-ply laminates. A number of different FOS exists, of which the Fibre Bragg Grating (FBG) and Extrinsic Fabry-Perot Interferometric (EFPI) sensors are most often applied to monitor the formation of residual stresses. An EFPI sensor measures strain through a change in cavity length, which is related to a phase change between the input/output signals and the reflection of the optical fibres (Figure 3.2) [3].

The FOSs are minimally disruptive when embedded parallel to the reinforcing fibres, provided that the thickness of the ply matches the diameter of the optical fibre and generally

they do not cause any degradation of macroscopic properties. This does not stand however when a FOS is embedded perpendicularly to the fibre direction. In that case, an eye-shaped defect is created, which causes a stress concentration and deterioration of the mechanical properties. One fibre often contains many sensors (Fibre Bragg Gratings) and therefore an array of FOSs can be embedded inside a laminate (“multiplexing”) and give information on the residual stress distribution throughout the laminate on a macro-mechanical as well as a global level. The strain resolution is higher than 1 με [3].

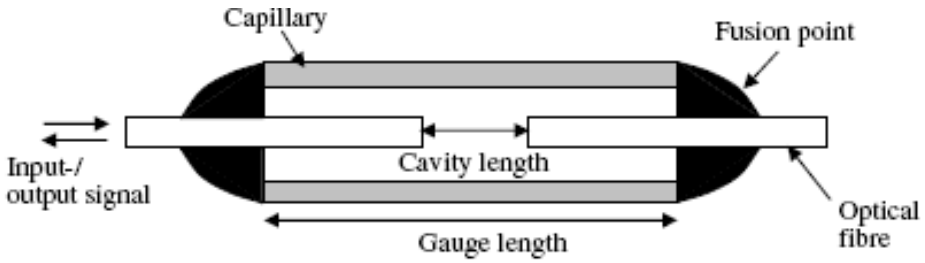

Figure 3.2: Schematic view of EFPI sensor (Figure from reference [3]).

3.2.3 Embedded metallic particles

This technique measures the deformation of a thermoset polymer matrix using the method of X-ray diffraction (explained in paragraph 3.3.4) on metallic particles which are embedded in the matrix. Aluminium, copper and silver particles present a deflection in peak angle, when they are embedded in composite materials. Using the Bragg's law, this deflection can be related to changes in the spacing of the crystal lattice due to the residual strains. The measured strain can be related to the residual stresses through the Hooke's law or via a stress transmission tensor. The regularly shaped aluminium particles provide the highest accuracy. This technique can measure through the thickness only in thin specimens (0.3-0.5 mm). For thick specimens, it can only provide information about their surface properties [3].

This method is mainly performed in thermoset matrices, since they do not have a crystalline structure which changes in response to X-rays when strained, and therefore thermosets need crystalline fillers. In semi-crystalline thermoplastics, the lattice spacing between the crystals and the change due to straining can be measured by means of X-ray diffraction. This was shown to be possible for polyetherketone (PEK) reinforced with carbon and glass fillers, but this technique was not yet tested for continuous fibre reinforced thermoplastics [1].

3.3 Methods based on in-plane and out-of-plane deformations

3.3.1 Methods based on interferometry

The interference of light waves reflected from an object creates an optical pattern which can be used for the determination of deformations. Some of the methods which use this interference phenomenon have been applied for the calculation of residual stresses in composite materials. The Moiré effect in optics is based on an interference pattern which develops when light passes through two gratings rotated at a small angle with respect to each other. When one of the gratings changes due to deformation of the sample, the resulting interference (Moiré) pattern will also change [3].

Moiré interferometry can be used to monitor both in plane and out-of-plane displacements. For in-plane displacements a grating should be applied on the surface of the specimen. For out-of-plane displacements, there is no need to apply a grid on the surface, since the grating can be projected onto the surface at an angle to the viewing direction [3].

The cure reference method was developed to measure the thermal residual strains on thermoset materials by the use of Moiré interferometry. It is a full-field laser method that monitors the development of strains on the surface of a composite laminate during cooling down. A grating is applied on the material during curing and acts as a reference to the stress free condition just prior to the stress free temperature. The result of the interference is a characteristic pattern of light and dark fringes, which can be used to determine the in-plane-displacements in symmetric laminates from which the residual stresses can be calculated utilizing lamination theory. The advantages of this method are that it provides a high level of accuracy on its results, is a non-contact full field method, it has high displacement and strain sensitivity, high spatial resolution and high signal to noise ratio. However, it provides information only for the strains on the surface of the specimen and an interference image needs to be captured when no strains are present, which may be difficult for thermoplastic composites [3].

3.3.2 Methods based on warpage of non-symmetric composite materials

A usual indication for the existence of residual stresses in non-symmetrical composites is the warpage. Therefore, a relatively simple method for the calculation of the magnitude of residual stresses is the measurement of out-of-plane deformations in non-symmetric or angle-ply laminates, knowing that the residual stresses can be relieved by these deformations. The monitoring of out-of-plane deformations may be performed during or after cooling from the processing temperature. The greater the curvature of a composite material with a specific thickness, the higher is the magnitude of the residual stresses [3]. The most common method for measuring the curvature is cutting the specimen in narrow strips and measuring both the deviation at the centre and the chord length. Using narrow strips makes the measurements easy since unlike the whole specimen there is only one dominant curvature. A disadvantage of the curvature method is that the results may deviate considerably for equal laminates under similar conditions. This can be explained by the limitations in the accuracy of curvature measurement, by non-symmetry of ply thickness, disorientation of the plies, as well as deviations in the alignment of the fibres. Additionally, this method does not provide any information for the spatial variation of residual stresses at the micromechanical level resulting from varying fibre distribution, variable thermal contraction, etc [1],[3].

3.3.3 Neutron diffraction

Neutron diffraction is a crystallographic method for the determination of the atomic and / or magnetic structure of a material. It is a form of elastic scattering where the neutrons exiting the experiment have more or less the same energy as the incident neutrons. This technique is similar to X-ray diffraction, only better since the different type of radiation provides complementary information. A sample to be examined is placed in a beam of thermal or cold neutrons and the intensity pattern around the sample gives information of the

structure of the material. One practical application of elastic neutron scattering / diffraction is that the lattice constant of metals and other crystalline materials can be very accurately measured. Together with an accurately aligned micro-positioner, a map of the lattice constant through the material can be derived. This can be easily converted to the stress field experienced by the material [1].

3.3.4 X-ray diffraction

X-ray diffraction is a method that can be applied to materials presenting a crystalline structure, and has been applied in the past for the determination of residual stresses in metal matrix composites. In the literature, variations of the method are described which may be applied for the determination of residual stresses in composites. In these cases nickel particles were introduced into the resin and then the X-ray diffraction was carried on these particles. Results were provided for nickel particles within cured resin rather than a fibre composite [11].

The X-ray diffraction method can measure residual stresses in crystalline materials to a maximum depth of about 0.05 mm. Measuring to a greater depth requires layer removal, such as by etching, and makes the measurements destructive [12]. According to reference [3] the thickness of a specimen with metallic inclusions, where the X-ray diffraction can measure through the thickness, is from 0.3 to 0.5 mm.

3.4 Estimation of residual stresses using destructive methods

The main disadvantage of the non-destructive methods described above is that they do not provide information for the distribution of global residual stresses in the composite or along the plies. The methods which can measure the distribution of residual stresses are based mainly on destructive techniques. The general principle shared by all destructive methods, is that some stressed material is removed and the resulting deformations (usually displacements or strains) are measured [13]. The destructive methods include: first ply failure, layer removal method, the incremental hole drilling method, the deep hole method and the crack compliance method. The method used in this study is the incremental hole drilling method, presented in section 3.4.5.

3.4.1 First ply failure

The thermal contraction in symmetric cross-ply composites causes the development of tensile residual stresses in the transverse (90°) plies. When the composite material is loaded in the transverse direction, its tensile strength $\sigma^{t}_{0/90}$ (t represents the transverse direction) has been found to be lower than the tensile strength of a similar unidirectional composite in the longitudinal (0°) direction $\sigma_{0/0}$. The tensile strength is calculated through acoustic emission of the first crack and therefore the term first ply failure comes up. The difference between the tensile strengths provides an approximation of the residual stresses between plies (interlaminar residual stresses) σ_R, where $\sigma_R = \sigma_{0/0} - \sigma^{t}_{0/90}$. The 90° plies are positioned at the external surface to ensure the noise of the cracking would not be suppressed [3].

3.4.2 Layer removal method

The methods described in this section are destructive relaxation based techniques. These techniques depend on the removal of some stress material and the measurement of the resulting strains. They were originally developed for isotropic materials such as metals but were modified properly for composites. By the use of these methods, both the calculation of the global residual stress distribution through the thickness and the determination of lamination stresses are possible.

In the layer removal method, abrasion or milling is employed to remove one or more plies of the composite material. The stresses released can be calculated through the measurement of the strains and the deformation which develops in the laminate after the material removal. Therefore, strain gauges are installed on the opposite side of the material removed, while the deformation can be measured by Moiré interferometry [3].

According to reference [3] this method lacks in accuracy. This occurs because during the layer removal the surface temperature rises and also microcracks are created, both of which lead to the relaxation of residual stresses. Moreover, the irregularities caused at the plies from abrasion, e.g. alteration of the thickness of the plies, affect the final shape of the resulting deformation. In order to avoid the creation of damage in the laminate during material removal, the Process Simulated Laminates (PSL) technique is used. PSL composite materials consist of prepreg plies and other thin separating films placed between the plies. The plies between two thin separating films constitute a laminate called constitutive laminate (CL) (Figure 3.3). These constitutive laminates may be removed from the composite material after manufacturing.

The calculation of residual stresses can be achieved by either of the two following techniques. Firstly, by the use of the constitutive laminate deformation technique, i. e. through the measurement of the dimension changes (curvature) of the PSLs and of the CLs before and after their removal. Secondly, by the PSL - strain gauge technique, where strain gauges are bonded on the surface of the composite, which monitor the strain changes as CL's are removed from the other side [3].

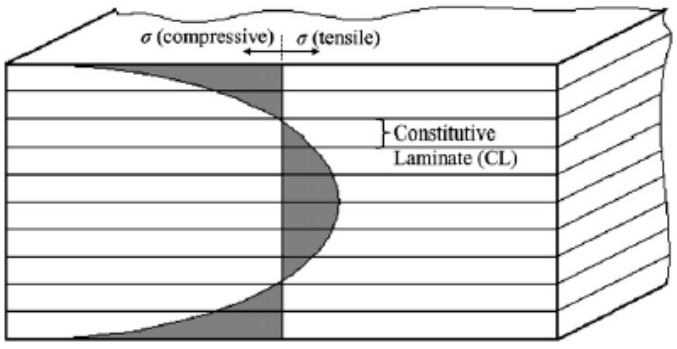

Figure 3.3: Schematic view of the process simulated laminate (PSL) configuration with constitutive laminates (CL) for determination of laminate skin-core residual stress distribution (grey area) trough this type of the layer removal method (Figure from reference [3]).

Both measuring techniques provide reliable results, with the PSL - strain gauge technique being more accurate. An important parameter of this method is the use of proper films for separating the layers. These films should achieve perfect bonding with the composite so that

the loads can be transferred and also they should separate easily from the composite after manufacturing. Furthermore, they should not affect the creation of residual stresses [3].

3.4.3 Deep hole method

The deep-hole method is used for the measurement of residual stress in isotropic materials, but it can be also applied to orthotropic materials such as thick laminated composites. It should be noted that for large structures this method is considered non-destructive, since a small hole does not affect the structural integrity. The deep-hole method bases its formulation on a calculation of the distortion of a hole in a plate subject to remote loading. For the isotropic case there are suitable closed-form solutions, however for the orthotropic case a finite element approach should be used [1].

In reference [11], the residual stresses in a 22 mm thick composite plate were calculated using the deep hole method. A composite plate was constructed using a resin film infusion process from plies of a carbon non-crimp fabric and epoxy film resin. Seven plies were laid up at the same orientation through the thickness of the specimen. The maximum magnitude of the calculated residual stresses was about 40 MPa in the fibre direction and 10 MPa in the transverse direction [11].

3.4.4 Crack compliance method

Another stress relaxation technique is the crack compliance method, which can be found in the literature as successive cracking method, the slotting method, and a fracture mechanics based approach [12]. In this method, a single slot or multiple slots (also called grooves or slits) are incrementally cut into a specimen. Deformations due to the relaxation of stresses are measured with strain gauges in order to determine the residual stresses through the thickness (Figure 3.4). This method is destructive, but does not require specific specimen preparation and offers a high degree of accuracy [3].

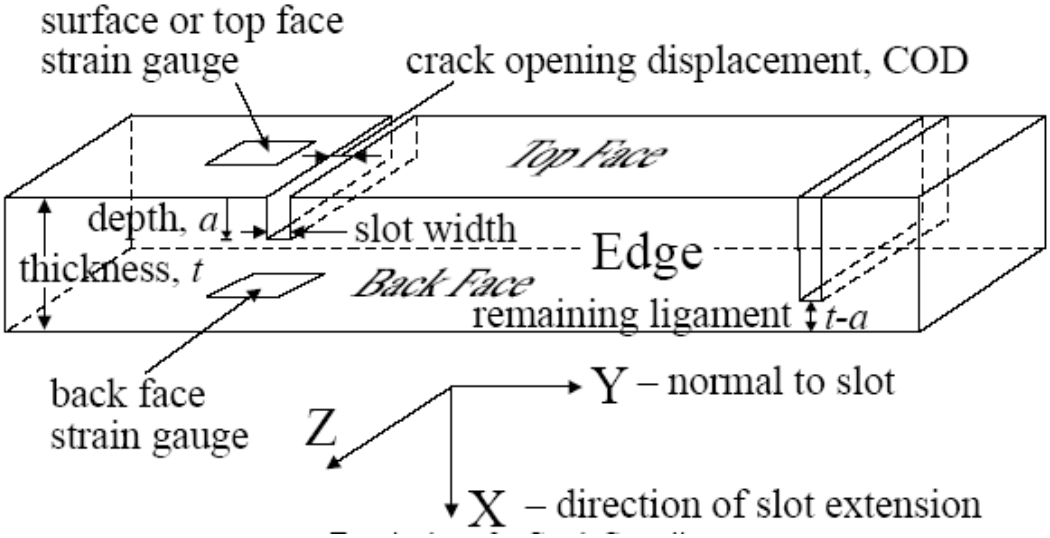

Figure 3.4: Terminology for crack compliance method (Figure from reference [14]).

Several techniques exist for implementation of the crack compliance method, such as the beam-bending approximation of Reid, the series expansion approach and the fracture mechanics approach. The authors of reference [15] state that the Reid's beam-bending

approximation is significantly inaccurate, while both the series expansion approach and the fracture mechanics approach work well, but having different advantages and disadvantages.

The fracture mechanics approach relies on the approximation of the slot, which was introduced for relaxation of the residual stresses, as a mathematical crack. This approximation was proven valid for a slot with a depth-to-width ratio greater than five. The residual stress results are generally accurate except for very deep cracks. The calculations require a weight function solution for the given geometry and differentiation of the measured strains, and therefore care must be taken to minimize errors. For near-surface measurements, where the ratio of slot depth to width is less than five, some errors may come up, since the method assumes a mathematical crack [15].

In the series expansion approach the residual stress profile is determined from the measured strains, with a technique originally developed for hole-drilling measurements. First the unknown residual stresses are written as a series expansion. Then the strains, which are called compliances, are calculated for each term (basis function) of this series. Finally, a least-squares fit is performed between the calculated strains and those measured, which provides the coefficients of the series expansion terms. Hence, the unknown residual stresses result from the series expansion equation. With this method, the residual stress profile can be determined quite accurately, with some limitations depending on the choice of the basis functions of the series. This approach is especially tolerant to strain measurement errors, and is simple to account for the finite width slot which allows for near-surface measurements [15].

3.4.5 Incremental hole-drilling method

For isotropic materials the most widely used method for the measurement of residual stresses is the hole drilling method. This method is based on the stresses released by drilling a small hole on the material. The dimensions of the hole and its geometry change due to the release of the stresses, because of the material removal. These changes result in deformation of the material surrounding the hole, relative to the undisturbed situation. The deformations can be measured with a strain gauge rosette. The hole is drilled at the centre of the strain gauge rosette, which is bonded on the surface of the composite material. This method was initially developed for isotropic and homogeneous materials. Nevertheless, it can be used for orthotropic materials too, through the introduction of proper calibration coefficients. These coefficients can be obtained by calculation or experimentation. In composite materials, residual stresses are not invariable through the plies (i.e. are not uniform through the thickness). For this reason, the hole drilling method was modified to the incremental hole drilling method, which can take into consideration the non-uniformity of the stress distribution through the thickness. The basic principle for the calculation of stresses is the same with the hole drilling method, but in this case drilling is performed gradually. The measured strains are processed by an appropriate model and the stresses present before the hole drilling are calculated [16, 3, 17].

A disadvantage of the hole drilling method is that the size of a typical strain gauge rosette is two to four times larger than the diameter of the hole, making the area covered by the rosette very large compared to the stress field. Also, a frequent problem of the hole drilling method is the eccentric drilling, i.e. when the hole is not drilled exactly at the centre of the rosette. The hole drilling method has been applied in combination with Moiré interferometry,

holographic interferometry and speckle interferometry, as well as in combination with finite element modelling for determination of the residual stresses. Incremental hole-drilling can be utilised to study residual stresses in between adjacent plies, but optimal drilling and translation speeds should be found [3].

The hole drilling method is carried out according to the ASTM E837 standard (“Standard Test Method for Determining Residual Stresses by the Hole-Drilling Strain-Gauge Method”). For large structures this method can be considered as non-destructive, since a small hole does not affect the structural integrity. Furthermore, it should be mentioned that since the distance between the strain gauges and the hole is small, the drilling has to be performed without significant plastic deformations and heating. Therefore, high speed drilling machines of 300.000 revolutions per minute are used or air abrasive particles [17].

In reference [18], the influence of the depth increment in relation to the ply thickness and the relative position of the strain gauge are examined for the determination of residual stresses in composite laminates. Choosing an increment that is too significant (for example one increment per ply) can lead to slight over-estimation of the residual stresses. This over-estimation is caused by a too significant stresses relaxation during and after the drilling. Indeed the larger the increment depth, the longer the drilling time and in this case it becomes possible that a damage will appear as microscopic cracks and would lead to a stress relaxation which comes over the residual stresses relaxation. By reducing the respective depth of each increment, the sensitivity of the method for determining the residual stress profile in the through-depth of the material can be increased. Furthermore, it was found out

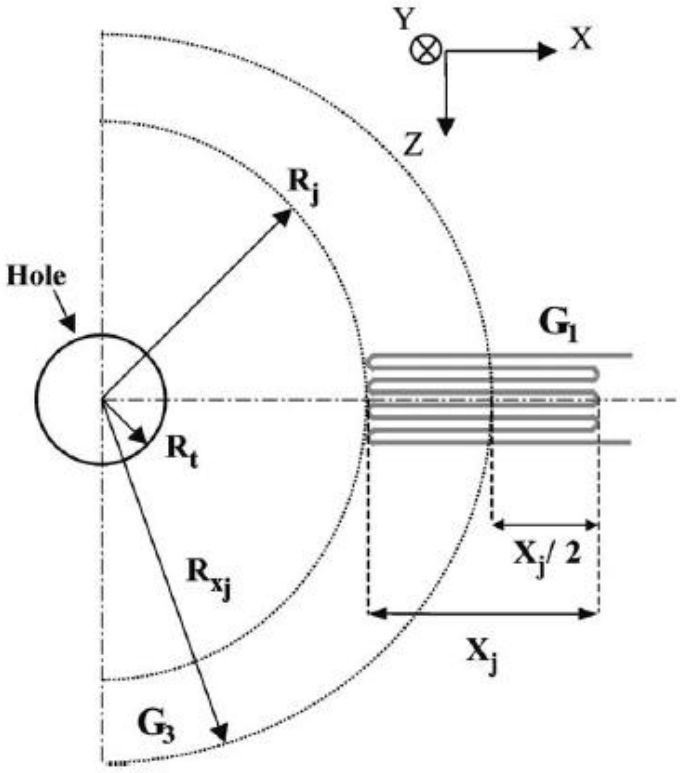

Figure 3.5: Relative location of the hole and the strain gauges (Figure from reference [18]).

that the relative gauge position plays a significant role in the quality and sensitivity of the residual stress calculations. It appears from the data tested that the best results are obtained

for the 0.30<δ<0.50 range of values. Outside this range, the residual stress calculated cannot be used. Also the λ ratio does not have any significant influence, which implies that the geometry of the gauge does not play an important role in the range of strain gauge lengths studied. The variables δ and λ (Figure 3.5) are defined as follows:

- δ is the ratio of the hole radius to the radius of the inside of the strain gauge ($\delta=R_t/R_j$).

- λ is the ratio of the hole radius to the radius of the middle of the strain gauge ($\lambda= R_t/R_{xj}$) [18].

This method was chosen for this study mainly for the following two reasons. Firstly, it can provide accurate results for the distribution of residual stresses through the thicknes of a composite material. Secondly, the necessary hardware was available at NTUA and the strain gauges and drill-bits needed were easy to acquire.

The following Tables 1 and 2 are from reference [3] and they present an overview of the main techniques for the measurement of residual stress.

Table 1
Overview of non-destructive experimental techniques for residual stress determination in composites

Technique	Level of residual stress			Type of specimen					Specimen requirements/ drawbacks
	Intraply stresses	Interply stresses	Laminate stresses	Micro-composites	UD prepregs	Cross-ply prepregs	UD laminates	Angle-ply laminates	
Photo-elasticity	X			X	X				Transparent matrix, low V_f
Raman spectroscopy	X	X, need aramid fibres in amorphous material		X	X		X		Transparent matrix, measures only fibre surface
Electrical conductance		X				X			In composites with electrically conducting fibres
Embedded strain gauges	X	X					X	X	Compensation needed for gauge CTE
Embedded FOS	X	X	X				X	X	Polarisation effects
Embedded metallic particles	X	X					X	X	Particles need to be close to surface
Interferometry		X					X	X	Only surface information, grid is necessary
Warpage		X			X	X	X	X	No high accuracy

Table 2
Overview of destructive experimental techniques for residual stress determination in composites

Technique	Level of residual stress			Type of specimen					Specimen requirements/ drawbacks
	Intraply stresses	Interply stresses	Laminate stresses	Micro-composites	UD prepregs	Cross-ply prepregs	UD laminates	Angle-ply laminates	
First ply failure		X				X		X	Works best for $[0/90]_{ns}$ laminates
Layer removal		X	X				X	X	No high accuracy
Blind-hole drilling		X	X				X	X	Low accuracy
Successive grooving technique		X	X				X	X	Low accuracy, time consuming

3.5 Finite element calculation of the residual stresses using the hole-drilling method

In this chapter, a method for the estimation of residual stresses from the measured strains will be presented based on the procedure described in references [16], [17], [19] as well as the assumptions of reference [20]. This procedure was used in reference [21] and is being currently employed for the estimation of the residual stresses from the strains measured during the experimental program of this study.

The radial strain at any location, for a fixed radial distance from the centre of the hole, can be described as follows:

$$\varepsilon_{in}(\theta_i) = A_{in}(\sigma_{1hi} + \sigma_{2hi}) + (\sigma_{1hi} - \sigma_{2hi})(B_{in}\cos 2\theta_i + C_{in}\sin 2\theta_i) \quad (1)$$

where ε_{in} is the strain contribution of layer i to the total strain measured on the surface for the nth increment, σ_{1hi} and σ_{2hi} are the principal residual stresses of layer i (the depth of the layer is h_i), θ_i is the angle between the reference gauge and the first principal direction of residual stresses, and A_{in}, B_{in}, C_{in} are the calibration coefficients for the nth increment when the ith layer is loaded. In our case the radial strains on the surface are measured by the three strain gauges of the 45º rosette (0º, 90º, 225º) for each increment.

For the nth increment the total depth becomes h_n and the strain contributions of this same layer n to the total measured strains on the surface, are:

$$\varepsilon^1_{nn}(\theta_n) = A_{nn}(\sigma_{1hn} + \sigma_{2hn}) + (\sigma_{1hn} - \sigma_{2hn})(B_{nn}\cos 2\theta_n + C_{nn}\sin 2\theta_n) \quad (2)$$

$$\varepsilon^2_{nn}(\theta_n) = A_{nn}(\sigma_{1hn} + \sigma_{2hn}) + (\sigma_{1hn} - \sigma_{2hn})(B_{nn}\cos 2(\theta_n + \alpha) + C_{nn}\sin 2(\theta_n + \alpha)) \quad (3)$$

$$\varepsilon^3_{nn}(\theta_n) = A_{nn}(\sigma_{1hn} + \sigma_{2hn}) + (\sigma_{1hn} - \sigma_{2hn})(B_{nn}\cos 2(\theta_n + \beta) + C_{nn}\sin 2(\theta_n + \beta)) \quad (4)$$

Where α and β are the angles of the 2nd and 3rd direction of measurement (i.e. the angles of the strain gauges).

For the 45º strain gauge rosettes which were used in the experiments, the following expressions can be derived from equations (2), (3) and (4), for the principal residual stresses and their direction:

$$\sigma_{1hn} = \frac{\varepsilon^1_{nn}(A_{nn} - B_{nn}\sin 2\theta_n + C_{nn}\cos 2\theta_n) - \varepsilon^2_{nn}(A_{nn} - B_{nn}\cos 2\theta_n - C_{nn}\sin 2\theta_n)}{2A_{nn}B_{nn}(-\sin 2\theta_n + \cos 2\theta_n) + 2A_{nn}C_{nn}(\sin 2\theta_n + \cos 2\theta_n)} \quad (5)$$

$$\sigma_{2hn} = \frac{-\varepsilon^1_{nn}(A_{nn} + B_{nn}\sin 2\theta_n - C_{nn}\cos 2\theta_n) + \varepsilon^2_{nn}(A_{nn} + B_{nn}\cos 2\theta_n + C_{nn}\sin 2\theta_n)}{2A_{nn}B_{nn}(-\sin 2\theta_n + \cos 2\theta_n) + 2A_{nn}C_{nn}(\sin 2\theta_n + \cos 2\theta_n)} \quad (6)$$

$$\theta_n = \frac{1}{2}\tan^{-1}\left[\frac{C_{nn}(\varepsilon^3_{nn} - \varepsilon^1_{nn}) - B_{nn}(2\varepsilon^2_{nn} - \varepsilon^1_{nn} - \varepsilon^3_{nn})}{C_{nn}(2\varepsilon^2_{nn} - \varepsilon^1_{nn} - \varepsilon^3_{nn}) + B_{nn}(\varepsilon^3_{nn} - \varepsilon^1_{nn})}\right] \quad (7)$$

However, the values of the three strains measured on the surface for the nth increment cannot be used directly for the estimation of the residual stresses at this increment, since the change of surface strains due to the removal of the previous layers should be considered too. Therefore, the following equations should be considered:

$$\varepsilon_{nn}^{1} = \varepsilon_{mn}^{1} - \sum_{i=1}^{n-1} \varepsilon_{in}^{1} \tag{8}$$

$$\varepsilon_{nn}^{2} = \varepsilon_{mn}^{2} - \sum_{i=1}^{n-1} \varepsilon_{in}^{2} \tag{9}$$

$$\varepsilon_{nn}^{3} = \varepsilon_{mn}^{3} - \sum_{i=1}^{n-1} \varepsilon_{in}^{3} \tag{10}$$

where ε_{mn}^{1}, ε_{mn}^{2}, ε_{mn}^{3} are the total strains measured on the surface by the strain gauges when the nth increment is removed, ε_{in}^{1}, ε_{in}^{2}, ε_{in}^{3} are the strain contributions of the ith layer while removing the nth increment, and ε_{nn}^{1}, ε_{nn}^{2}, ε_{nn}^{3} are the strains that should be used in equations (5), (6) and (7) for the estimation of the principal stresses and principal direction at the nth increment.

For the determination of ε_{in}^{1}, ε_{in}^{2}, ε_{in}^{3}, the following equations should be used:

$$\varepsilon_{in}^{1}(\theta_i) = A_{in}(\sigma_{1hi} + \sigma_{2hi}) + (\sigma_{1hi} - \sigma_{2hi})(B_{in}\cos 2\theta_i + C_{in}\sin 2\theta_i) \tag{11}$$

$$\varepsilon_{in}^{2}(\theta_i) = A_{in}(\sigma_{1hi} + \sigma_{2hi}) + (\sigma_{1hi} - \sigma_{2hi})(B_{in}\cos 2(\theta_i + \alpha) + C_{in}\sin 2(\theta_i + \alpha)) \tag{12}$$

$$\varepsilon_{in}^{3}(\theta_i) = A_{in}(\sigma_{1hi} + \sigma_{2hi}) + (\sigma_{1hi} - \sigma_{2hi})(B_{in}\cos 2(\theta_i + \beta) + C_{in}\sin 2(\theta_i + \beta)) \tag{13}$$

Where α and β are the angles of the 2nd and 3rd direction of measurement (i.e. the angles of the strain gauges). In equations (11), (12) and (13), the residual stresses σ_{1hi}, σ_{2hi} and the angle θ_i have already been calculated for the previous layers of increment n, and therefore the only unknowns are the calibration coefficients A_{in}, B_{in}, C_{in}.

The unknown calibration coefficients A_{in}, B_{in}, C_{in} can be determined by finite element analysis which simulates the incremental hole drilling process. For the calculation of the A_{in} calibration coefficients, a uniform stress (uniform pressure) should be applied at the hole boundaries of each increment in the finite element model. The coefficients A_{in} are then calculated by the following equation:

$$\mathrm{A}_{in} = \frac{U_{in}(r_2, \theta_n = 0) - U_{in}(r_1, \theta_n = 0)}{2\sigma L} \tag{14}$$

where r_2 is the outer diameter of the rosette strain gauges, r_1 is the inner diameter of the rosette strain gauges, $L=r_2-r_1$ is the gauge length, σ is the magnitude of the applied stress (pressure) and U_{in} is the radial displacement on the surface calculated by the finite element analysis.

For the calculation of the B_{in} and C_{in} calibration coefficients, a normal stress equal to $+\sigma\cos 2\theta$ and a shear stress equal to $-\sigma\sin 2\theta$ should be applied simultaneously at the hole boundaries of each increment. This biaxial stress distribution is presented in Figure 3.6 [20].

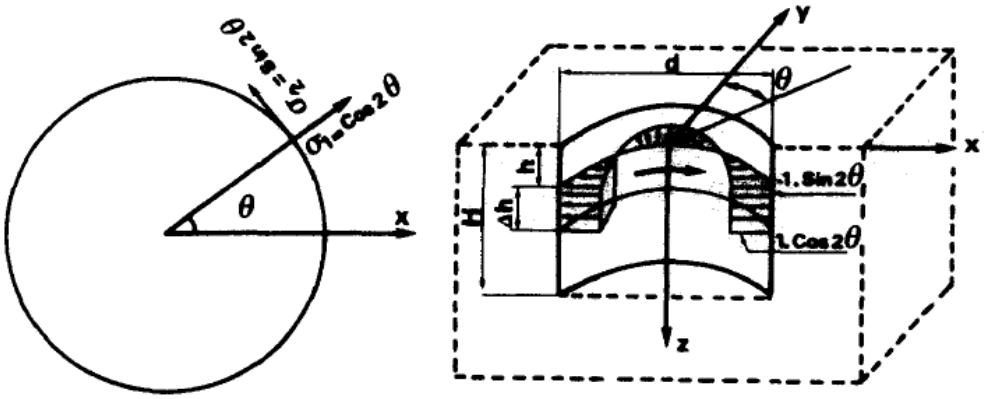

Figure 3.6: Biaxial stress distribution for the calculation of the calibration coefficients B_{in} and C_{in} (Figure from reference [20]).

The coefficients B_{in} and C_{in} are calculated by the following equations:

$$B_{in} = \frac{U_{in}\left(r_2, \theta_n = \pi/2\right) - U_{in}\left(r_1, \theta_n = \pi/2\right)}{2\sigma L} \tag{15}$$

$$C_{in} = \frac{U_{in}\left(r_2, \theta_n = \pi/4\right) - U_{in}\left(r_1, \theta_n = \pi/4\right)}{2\sigma L} \tag{16}$$

Where r_2 is the outer diameter of the rosette strain gauges, r_1 is the inner diameter of the rosette strain gauges, $L=r_2-r_1$ is the gauge length, σ is the magnitude of the applied stress and U_{in} is the radial displacement on the surface, calculated by the finite element analysis [21].

4. SPECIMENS AND EXPERIMENTAL PROCEDURE

4.1 Materials and material properties

4.1.1 Materials

In this work, materials that are typically used in the shipbuilding industry were chosen. The specimens were manufactured using epoxy or polyester resins with a combined glass fibre cloth which consisted of both woven roving and chopped strand mat. Specifically the following materials were used:

a. D.E.R. ™ 353 liquid epoxy resin from Dow Chemical Company ("Dow")
b. Epamine PC13 curing agent for epoxy systems from PO.INT.ER S.r.l.
c. PE-6/TC polyester resin
d. Appropriate hardener (MEKP 50) for the polyester
e. Agimat WRM-600.300/125 cm glass fibre, which is a 600 g/m^2 woven roving combined with a 300 g/m^2 chopped strand mat.

In order to investigate how the choice of the materials and the fabrication method affects the level of the residual stresses in a composite structure, five different laminate layups were considered for this study. For the glass-epoxy laminates two different fabrication methods were used, vacuum bagging and hand layup. For each fabrication method two different curing cycles were applied. In the cold cured case the structure was left to cool down at ambient temperature at 25 ºC. In the post cured case the structure was left for 24 hours at 25 ºC , then it was heated at 100 ºC for two hours and finally was left to cool down at 25 ºC at ambient conditions. The glass-polyester structure's fabrication method was hand lay up and was left to cool at 25 ºC for 24 hours. The curing temperature of 25 ºC was suggested by the resin manufacturer both for the epoxy and the polyester, while the post curing cycle was chosen taking into consideration the requirements of the hardener used in this particular study. Furthermore, for the vacuum bagging construction cases, the vacuum was set at 80%

So, five different composite material structures were finally manufactured, as follows:

a. Epoxy resin, Agimat WRM-600.300, hand lay up (HLU), cold cured (Case "A").
b. Epoxy resin, Agimat WRM-600.300, hand lay up, post cured (Case "B").
c. Epoxy resin, Agimat WRM-600.300, vacuum bagging, cold cured (Case "C").
d. Epoxy resin, Agimat WRM-600.300, vacuum bagging, post cured (Case "D").
e. Polyester resin, Agimat WRM-600.300, hand lay up, cold cured (Case "E").

According to the ASTM –E837 "Standard test method for determining residual stresses by the hole-drilling, strain-gauge method" of 1999 and 2001 the relief of the residual stresses is nearly complete when a hole depth of 40% of the mean diameter D of the strain gauge is reached. In the present study the chosen drill bit has a 3.2 mm diameter and the corresponding strain gauge mean diameter is about 10.8 mm therefore, the relief of the residual stresses is nearly complete at a depth of 0.4 x 10.8 = 4.32 mm. This standard mentions that for specimens with a thickness of about 0.4D the hole should be drilled throughout the thickness of the specimen. In the present study, the thickness is 4-5 mm which is about 0.4D (4.32 mm). It should be mentioned that in this standard, the procedure for determining residual stresses near the surface of isotropic linearly-elastic materials is covered, and it is applicable in those cases where the stresses do not vary significantly with

depth. This is not valid in the present case since a GRP material is used which is orthotropic and the stresses vary significantly with depth.

It was decided for the holes to be drilled through the thickness of the specimens, in order for the change of strain readings to be recorded through the thickness, but also in accordance to the provisions of the above-mentioned standard, that suggested when the thickness of the material is equal or less than 0.4D the hole is to be drilled throughout the specimen, since no other standard was found to cover orthotropic materials with depth varying residual stresses.

Thus, since a 3.2 mm drill bit was chosen for the hole drilling process, the number of layers for each structure was chosen so that the thickness is kept between 4 mm and 5 mm and therefore the residual stresses are estimated throughout the thickness of the structure. So, for the hand layup cases 4 layers were used, while for the vacuum bagging cases 6 layers were used. The average layer thickness was calculated by dividing the thickness of the plates constructed for the preliminary experiments by the number of layers for each case. This way, the number of layers to be used for the specimens was determined in order to achieve the desired thickness. The average thicknesses of the structures after the construction were:

a. Case “A”: 4.64 mm (4 layers)
b. Case “B”: 4.64 mm (4 layers)
c. Case “C”: 4.8 mm (6 layers)
d. Case “D”: 4.8 mm (6 layers)
e. Case “E”: 4.16 mm (4 layers)

All the composite structures were symmetrically constructed, so half of the layers had the chopped strand mat facing down while the other half had the chopped strand mat facing up.

4.1.1 Determination of material properties

Since there is no data of the material properties of the specific materials used for this work they had to be determined experimentally. The obtained results are required for finite

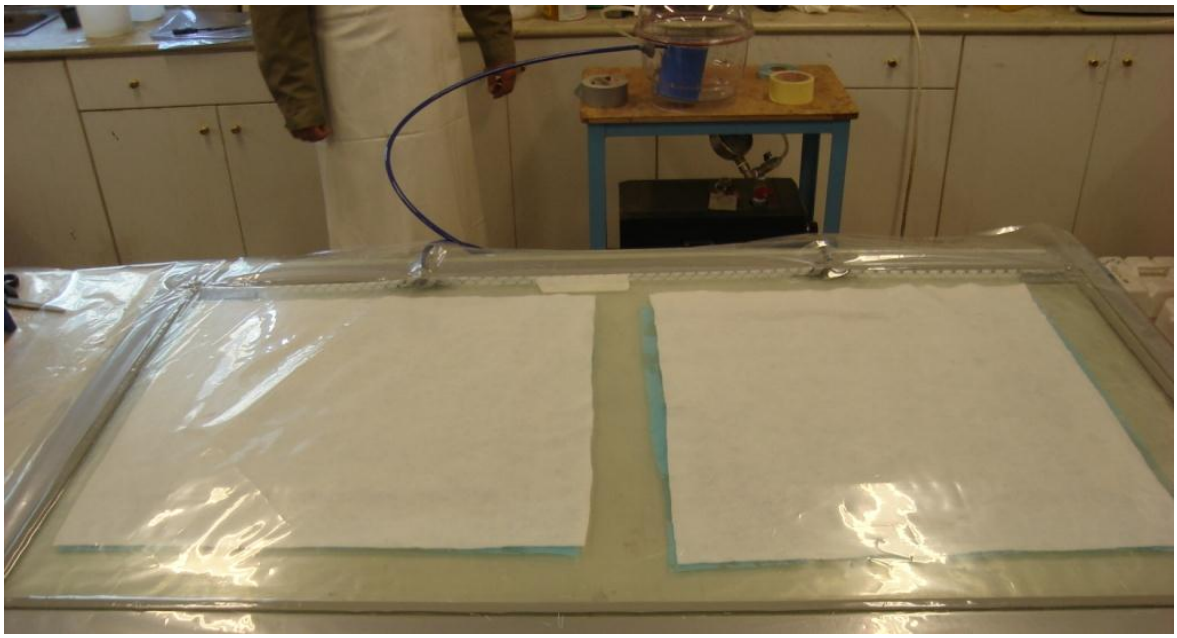

Figure 4.1: Vacuum bagging of the flat plates before suction is applied.

element models simulations, which are necessary for the determination of residual stresses from the measured strains.

In order to conduct these experiments, specimens had to be constructed for each different material (cases A-E).Five square flat pieces (400 mm x 400 mm) were therefore constructed. For each case the structure constructed on the tool for the residual stresses calculation and the flat plate for the properties estimation were to be made simultaneously. This way it was assured that both the structure and the flat plate would be constructed and cured under the same humidity and temperature. Therefore, the properties that would be measured on specimens cut from the flat plates would not differ due to environmental conditions from the actual properties of the structure. This could not be applied to the vacuum cases (C & D) because it was not possible with the given equipment, since with only one vacuum pump to use, it was impossible to apply vacuum in both the plate and the specimen before the gel time of the resin expired. In all cases an AC unit was used to keep the ambient temperature at 25 ºC and the humidity levels at~ 40%. The temperature was chosen from the resin's data sheet. Figures 4.1 and 4.2 show the construction of vacuum bagging plates before and after the vacuum was applied, respectively.

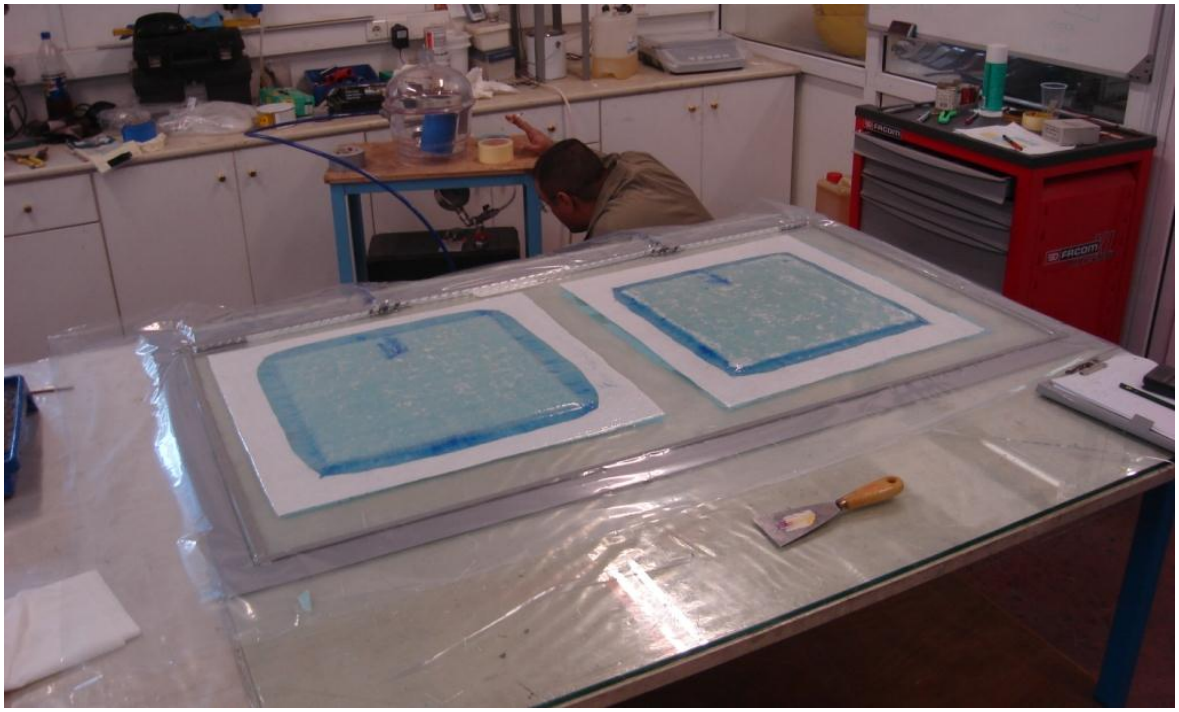

Figure 4.2: Vacuum bagging of the flat plates after suction is applied.

For each case six specimens were cut for the determination of the tensile properties of each material. This way after statistical analysis of the results more accurate values of the tensile properties can be obtained. Before the cutting they had to be marked on each plate with a marker. The cutting took place on a disk cutter which was constantly cooled with water. This way the edges were clean and the fibres and resin around the cut were not affected by the heat of friction. After the cutting more marking took place. Lines were drawn to show the area were the grips of the testing machine would attach on the specimen. Another line was drawn on the centre of the specimen in order to help attach and centre the extensometer for measuring strains. The dimensions of the specimens that were cut out of the plates were 250 mm long and 25 mm wide according to the ISO standard 527-4:1997

(type 2 specimens). The grips of the testing machine would need 50 mm length on the specimen, so the distance between the grips was 150 mm (Figure 4.3).

The last step before the conduction of the experiments was the exact measurement of the dimensions of each specimen. The width and the thickness were measured on five different places on each specimen in order to get their mean values. This way the cross section area of each specimen could be calculated by multiplying the thickness times the width of each specimen.

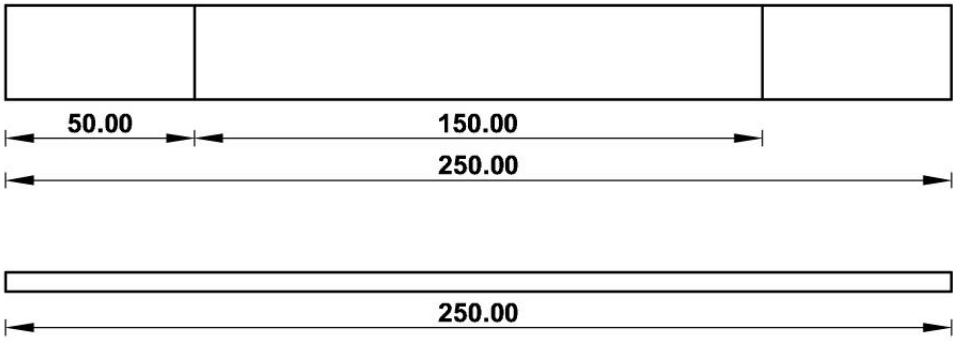

Figure 4.3: Drawing of the specimen for the tensile testing of the materials.

The testing machine where the tension experiments were conducted (Figure 4.4) was connected to a data acquisition device. The sampling frequency was 5 Hz. The data recorded was the applied force and the elongation. Furthermore, an extensometer was fitted on the specimen so that the strain is also measured and recorded.

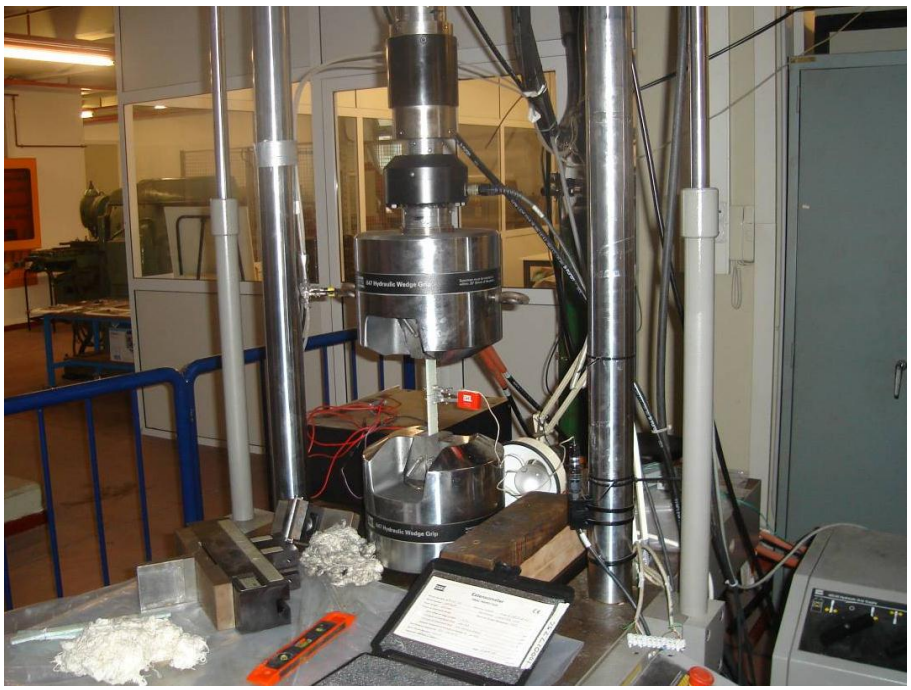

Figure 4.4: The tensile testing machine.

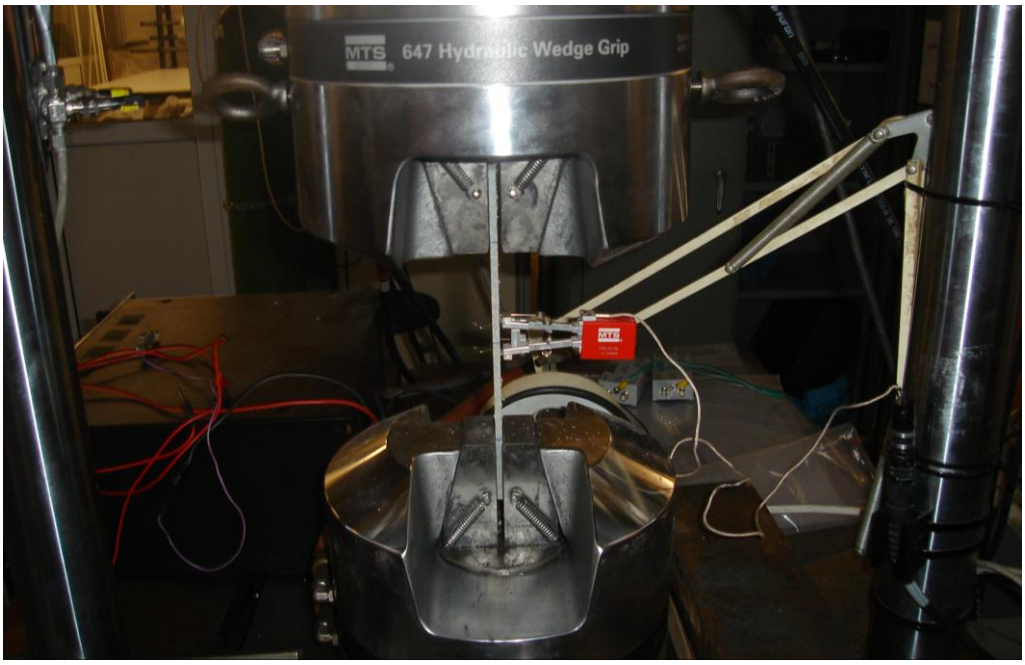

Figure 4.5: A specimen on the tensile testing machine before the test.

The pressure on the grips was manually set to 8 MPa for HLU specimens and 10 MPa for vacuum specimens. It was chosen so as not to cause damage to the specimens or create a stress concentration area where the specimens could fail during the test, thus affecting the measurements. It was also important that the grips should be firm enough in order to prevent the specimen from slipping during the test. Each specimen was positioned in the grips using

Figure 4.6: A specimen on the tensile testing machine after the test

the marking that was done earlier and was also aligned to the vertical axis using a spirit level. Finally, the extensometer was fitted on the centre of the specimen and connected to the data

acquisition system and the first value of all measurements was set to zero. Figure 4.5 shows a specimen positioned on the machine before the test, where the extensometer (red device) is also visible.

After all the preparation was done the tension test could start. The machine would apply force to the specimen using a hydraulic system which would keep a steady testing speed. Testing speed is the speed of the two grips moving apart, thus straining the specimen. The testing speed was selected to be 2 mm/min for the HLU specimens and 1 mm/min for the vacuum construction specimens. Each test stopped once the specimen failed, so the duration of the test depended on the material of the specimen and was about the same for specimens made out of the same material. It should be noted that throughout the test, the testing personnel wore breathing masks. This safety measure was taken in order to prevent the testing personnel from breathing in small particles of the specimen that may have broken off when it failed, particularly during the removal of the specimen and the positioning of the next one. Figure 4.6 shows a specimen that failed still positioned on the machine.

After each test was carried out the results were firstly saved on a .dat file (raw data) and then imported on an .xls (Microsoft excel format) file where their processing could take place. The data appeared in four columns: time (s), displacement (mm), force (kN) and strain. At the Microsoft excel file, the force was divided by the cross section area of each specimen, which was measured before the test in order to get a fifth column showing the stress values. The maximum stress value was the tensile strength of the specimen. Then a stress-strain

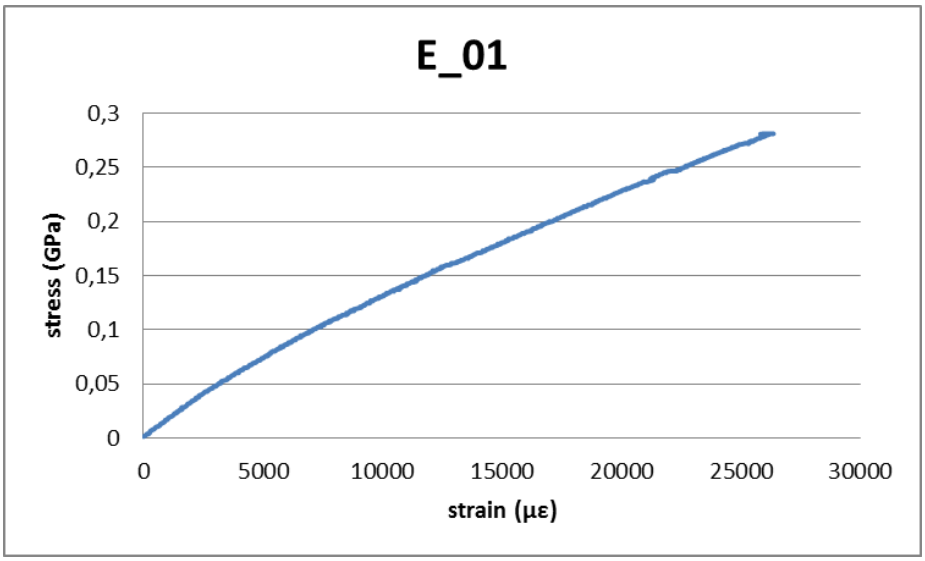

Figure 4.7: Stress-strain diagram for specimen 1 of case “E” (polyester HLU)

diagram was plotted from the zero value to the maximum stress value. Figure 4.7 shows a stress-strain diagram as an example. The shape of the curve provides an indication for the correctness of the measurements.

Furthermore, the modulus of elasticity in tension was determined as suggested in the ISO 527-4: 1997 standard. Specifically, the slope of the graph was calculated in the area between 500 με and 2500 με. This was done by isolating this part of the graph and then applying a linear regression line (Figure 4.8). The slope of this line is the modulus of elasticity. In the case that the slope of the line seems irregular at the specified area, an appropriate part of the graph with the same length (2000 με) would be selected in an area where the curve would appear to be acceptable. This new area would be as close as possible to the first one

as possible so that its slope would still provide an accurate value for the modulus of elasticity. The value of R^2 (mean square error) was also calculated and if this value was close to 1 then the calculation of the modulus of elasticity was deemed accurate.

After the tensile strength and the modulus of elasticity in tension were calculated for all the specimens, statistical analysis was done in order to determine the final values for the

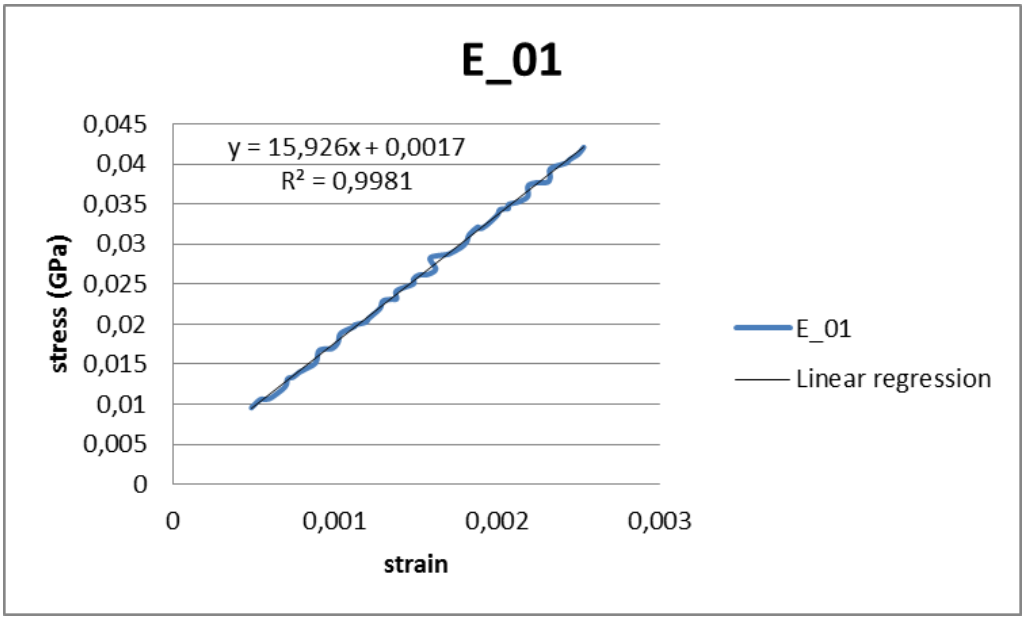

Figure 4.8: Stress-strain diagram for the calculation of the modulus of elasticity of the specimen 1 of case "E" (polyester HLU).

tensile strength and the modulus of elasticity in tension for the five different materials, cases "A" through "E". Specifically, the mean values, the standard deviation and the coefficient of variation were calculated. In all the results the coefficient of variation was under 5% which is a relatively small value, thus confirming the accuracy and repeatability of the test results. Table 4.1 shows the results for the tensile strength (σ_{M1}) in MPa and table 4.2 shows the results for the modulus of elasticity in tension (E_1) in GPa. The stress-strain diagrams for all specimens are presented in Appendix A.

Table 4.1: Table of results for the tensile strength (σ_{M1}) in MPa.

	σ_{M1}(MPa)				
	A	B	C	D	E
1	281.735	256.193	361.649	380.526	281.250
2	250.769	268.822	352.95	369.348	273.692
3	278.845	245.767	352.922	337.574	264.285
4	270.544	260.227	369.886	364.582	269.827
5	278.152	273.063	346.430	348.104	266.822
6	270.751	269.419	328.897	354.007	276.021
average	**271.799**	**262.249**	**352.122**	**359.024**	**271.983**
standard deviation	11.258	10.237	13.996	15.520	6.255
COV(%)	4.142	3.904	3.975	4.323	2.300

Table 4.2: Table of results for the modulus of elasticity in tension (E_1) in GPa.

	E_1(GPa)				
	A	B	C	D	E
1	13.467	12.395	16.721	16.532	15.926
2	13.185	12.989	16.874	17.716	15.689
3	11.885	12.561	17.348	17.170	15.919
4	13.500	12.690	16.595	17.203	14.782
5	12.647	12.326	17.033	16.849	15.811
6	13.101	12.851	17.124	16.407	15.368
average	**12.964**	**12.635**	**16.949**	**16.980**	**15.583**
standard deviation	0.612	0.258	0.276	0.485	0.443
COV(%)	4.721	2.044	1.626	2.853	2.843

The modulus of elasticity and the tensile strength values obtained from the experiments presented a coefficient of variation that was low for each type of specimen (under 5% in all cases). This proved the accuracy of the results and the repeatability of the experiments. Furthermore, by carefully studying the results the following conclusions are reached. In both the modulus of elasticity and the tensile strength the vacuum bagging construction specimens (cases “C” and “D”) present higher values. This variation occurs mainly because of the two more layers of glass fabric present in these specimens compared to the other construction methods. Another reason is the higher percentage of glass compared to the HLU construction specimens that was expected since the vacuum bagging construction method was used. The E_1 and σ_{M1} values for each case were virtually not affected by the post curing process, since the small difference in the results between the post curing and the cold cured specimens of each construction method is well within the standard deviation of each type of specimen. Case “E” specimens presented tensile strength measurements similar to the epoxy HLU specimens, as expected since the same number of layers of fabric was used in these cases. On the contrary, the modulus of elasticity in case “E” was significantly higher than the epoxy HLU cases. This variance is a result of the difference between the polyester and the epoxy resin’s material properties. Furthermore, the difference in the glass percentage between epoxy HLU and polyester HLU specimens is also a result of the difference between the polyester and the epoxy resin’s material properties since polyester resins shrink more during curing compared to epoxy resins.

The percentage of fibres by weight was also calculated according to the ISO standard 1172:1996(E). Two small square pieces (approximately 10 mm x 10mm) were cut out of each plate. Each one of them was then placed in a small metal container whose weight was measured beforehand (m_1). The metal containers with the small pieces were then weighted (m_2) and placed in the oven at 600 ^{o}C for two hours. This way the resin evaporated and only fibres remained in the containers. The containers were then weighted once more (m_3), this time containing only the fibres. Then with the use of the following equation (17) the glass content M_{glass}, expressed as a percentage of the initial mass was calculated. The final result for each material was the average of the two as shown in table 4.3.

$$M_{glass} = \frac{m_3 - m_1}{m_2 - m_1} \times 100 \quad (17)$$

Table 4.3: Table of results for the glass content.

Specimen No	m_1(g)	m_2(g)	m_3(g)	M_{glass} (%)	M_{glass} (%) average
A-1	77.3785	78.1548	77.7618	49.4	48.6
A-2	77.016	77.7959	77.3886	47.8	
B-1	76.5731	77.3924	76.9657	47.9	48.4
B-2	77.9163	78.7201	78.3085	48.8	
C-1	43.3814	44.403	44.0266	63.2	63.5
C-2	78.1026	79.1981	78.8011	63.8	
D-1	76.8835	77.752	77.4635	66.8	64.8
D-2	77.3943	78.361	78.0018	62.8	
E-1	45.5638	46.3478	45.9807	53.2	53.1
E-2	44.3172	45.0852	44.7249	53.1	

4.2 Preliminary experiments

Before the start of the actual hole drilling measurements, there were still some experimental parameters to be determined. The main variable to consider was the drilling speed and the resulting quality of the drilled hole. Another concern was the fastening method of the hole drilling device on the composite structure. In order to determine the values of these parameters three small flat composite plates were manufactured. The first one was a polyester-hand layup plate (case “E”) and the other two were epoxy cold cured hand layup (case “A”) and epoxy cold cured vacuum bagging plates (case “C”). It is considered that the post curing process does not significantly affect the quality of the hole and therefore no post cured plates were manufactured at this point.

Figure 4.9: Hole drilling hardware.

With the use of the existing NTUA hardware (DeWalt power drill and struers hole-drilling apparatus as seen in Figure 4.9), four different speeds were tested with a 3.2 mm drill bit and

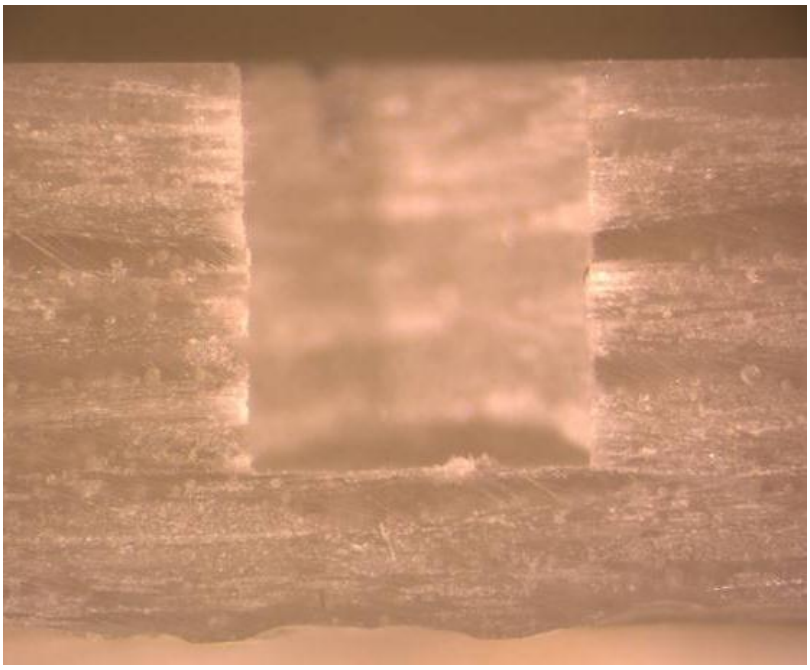

Figure 4.10: Manual drilling by hand

one with a 1.6 mm drill bit. The 1.6 mm diameter hole was drilled with an air turbine at 300,000 rpm. The diameter of this hole was 1.6mm because the air turbine was not compatible with the 3.2 mm drill bits. Despite the air cooling in this case, a friction burn was

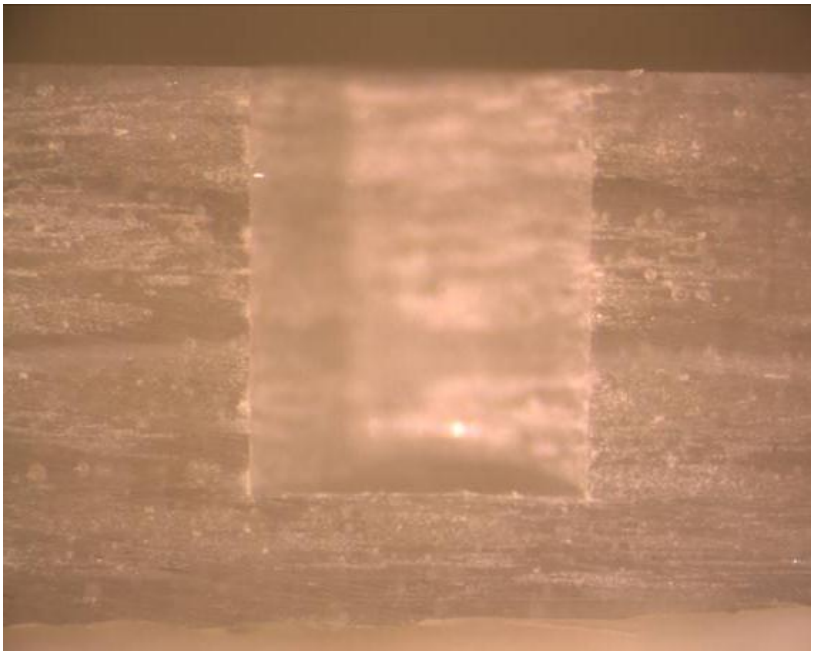

Figure 4.11: Electric drilling at 300 rpm

obvious around the hole so this method was not considered further. For the drilling of the 3.2

mm holes the methods included manual drilling by hand, electric drilling at 300 rpm, electric drilling at 1100 rpm and finally electric drilling at 2800 rpm. The electric drilling was performed with a handheld electric drill. The last case at 2800 rpm was not considered further either, because of excessive vibrations of the hole drilling equipment. The temperature around the hole area was measured using a laser thermometer during the drilling, but only small variations in temperature could be measured.

For each of the different drilling speeds, holes were made on the composite plates. After the drilling of the holes, the plates were cut with a disc cutting machine through the diameter of each hole and then pictures of the hole cross section were taken at the stereoscope in order to assess the quality of each hole and therefore determine the optimum drilling speed. Samples of the photographs can be seen in Figures 4.10-4.12.

By comparing the white areas surrounding the holes in Figures 4.10 – 4.12 it can be concluded that in the last case these areas are less and therefore the area surrounding the hole is less affected. In Figure 4.10 small white areas surrounding the cut are clearly visible at greater extent than the others. These white areas are assumed to be an indication of microcracks caused by the slow drilling speed. After carefully inspecting the photographs and paying special attention to the edges of the cut, the use of the 1100 rpm electric drilling was selected since the quality of the surface of the hole was better.

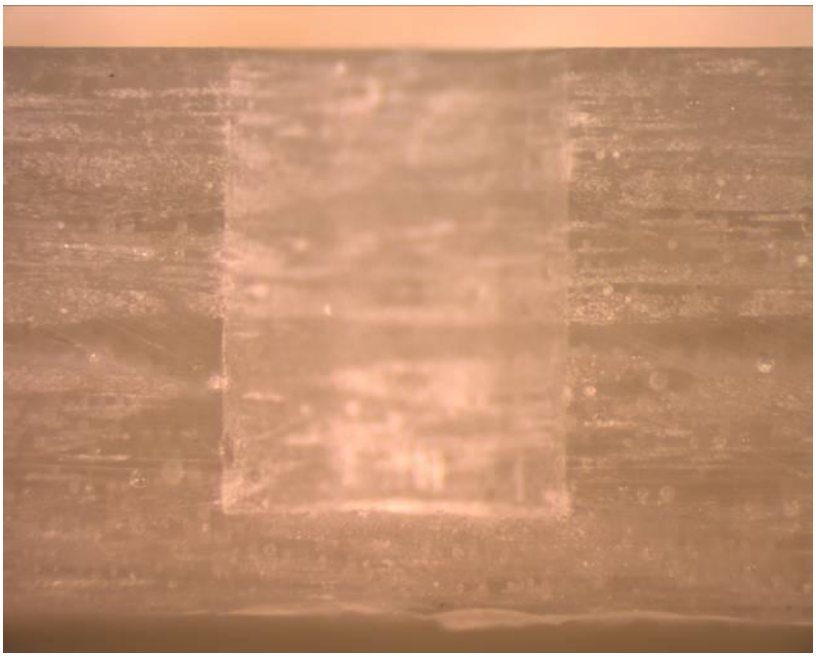

Figure 4.12: Electric drilling at 1100 rpm

In the third small composite plate strain gauges were also installed. The KYOWA 45º strain gauge rosettes (0°, 90°, 225°) were used (3 mm gauge length, 120 Ω gauge resistance). These rosettes were compatible with the 3.2 mm drill bit used in this study. Figure 4.13 shows a strain gauge rosette. The use of the strain gauge rosette revealed that when using clamping devices to fasten the hole drilling equipment onto the plate to be measured, the initial stain measurements before the drilling of the hole were raised significantly. This revealed a possible deformation of the composite plate caused by the tightening of the clamping devices. Therefore, it was decided that the hole drilling equipment should be glued on the surface of the composites. Furthermore, it was decided to fully retract

the drill from the device after each increment in order to get measurements that are not affected by its weight.

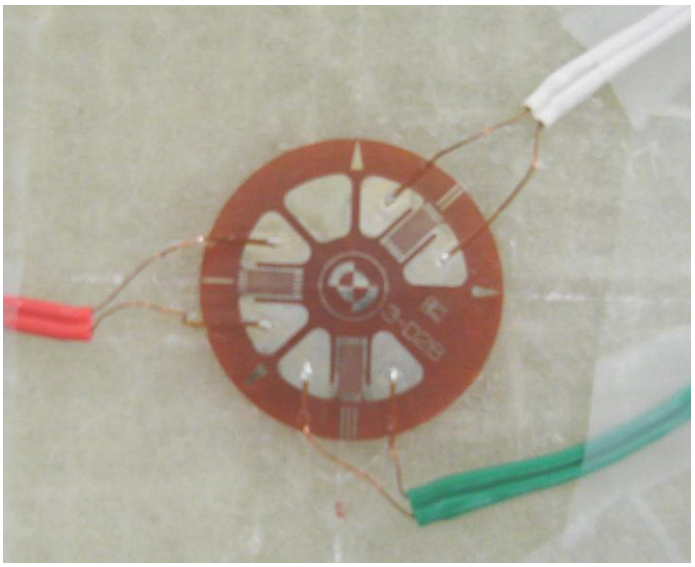

Figure 4.13: A 0º, 90º, and 225º rosette.

These preliminary experiments served another very important purpose. They helped the team get acquainted with the equipment and all the instruments. It helped in fine-tuning the experimental procedure, in choosing the right area to work and also in obtaining accurate estimations of the time each drilling would take.

4.3 Experimental procedure

4.3.1 The Tool

During the early stages of this study the shape and the material of the tool that would be finally used was discussed. The aim was to apply restrictions to the chemical shrinkage and

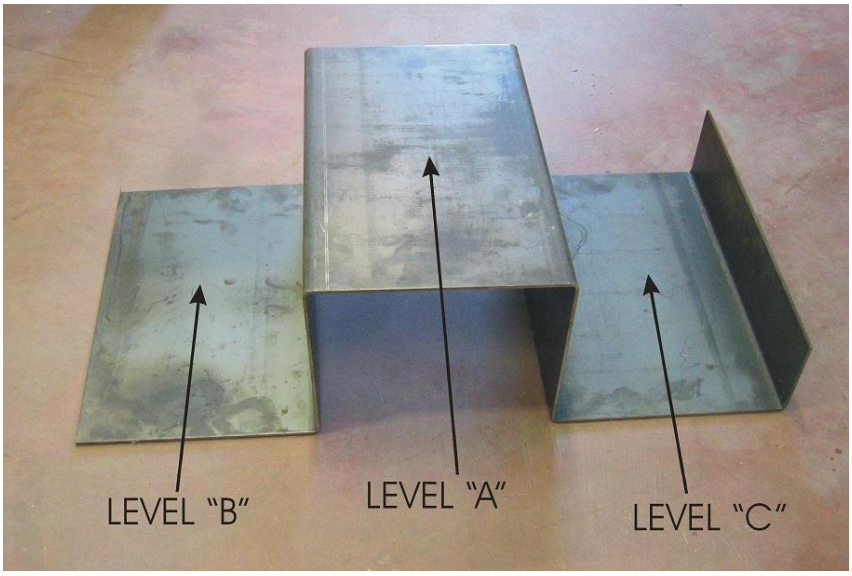

Figure 4.14: Tool imposing restrictions in the contraction – expansion of a composite structure during curing

thermal expansion of the composite structure that happen during curing. This way a higher level of residual stresses was expected to be measured on the composite structure. Furthermore, the tool should have three zones with different geometrical restrictions to the

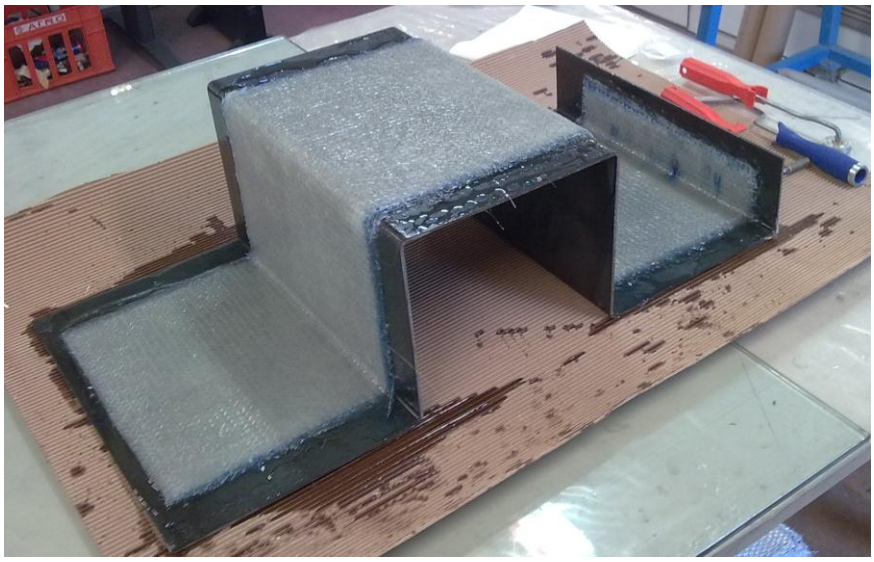

Figure 4.15: Hand layup construction.

structure's shape changes. Using this shape, three different residual stresses levels were expected to be measured on the structure. The highest level of stresses was expected to be measured at Level "A" which would apply constraint to shrinkage, more specifically, the chemical shrinkage that takes place during the vitrification of the resin (see Figure 2.3). Level "C" would apply constraint to expansion and level "B" would be the control area of the structure with no constraints to either shrinkage or expansion (see Figure 4.14). Figure 4.15

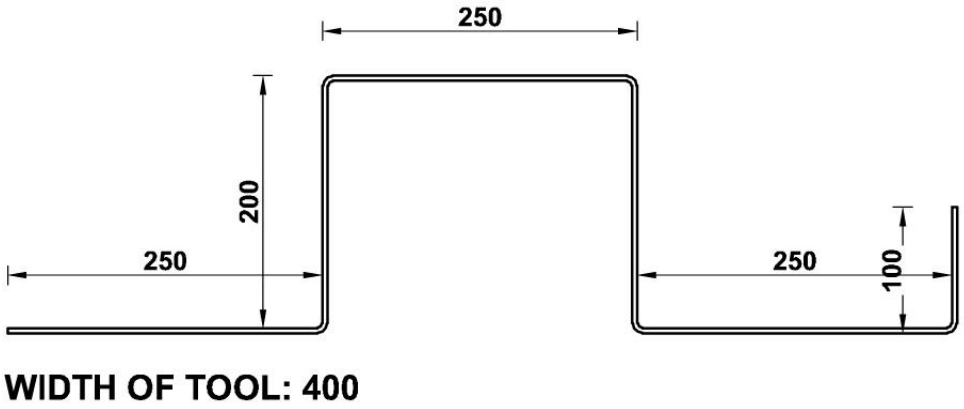

Figure 4.16: Dimensions of the tool in mm.

shows a hand lay up construction on the tool.

The material and the dimensions of the tool were determined next. The material should be sturdy enough so as not to deform during cold curing and more importantly during post

curing at 100 ºC. It should also be suitable for vacuum bagging. Thus, it was decided that the tool should be made out of a 4 mm steel plate formed on a press to the desired shape. The dimensions of the tool were restricted by the dimensions of the existing post curing oven at NTUA. The tool was large enough to manufacture a structure where more than one measurement on each level could be taken, but small enough to fit in the post curing oven. There was also enough space for the vacuum bagging films and tape to be applied. The final dimensions are shown in Figure 4.16. Figure 4.17 shows a vacuum construction, where the vacuum films and sealant tape are clearly visible.

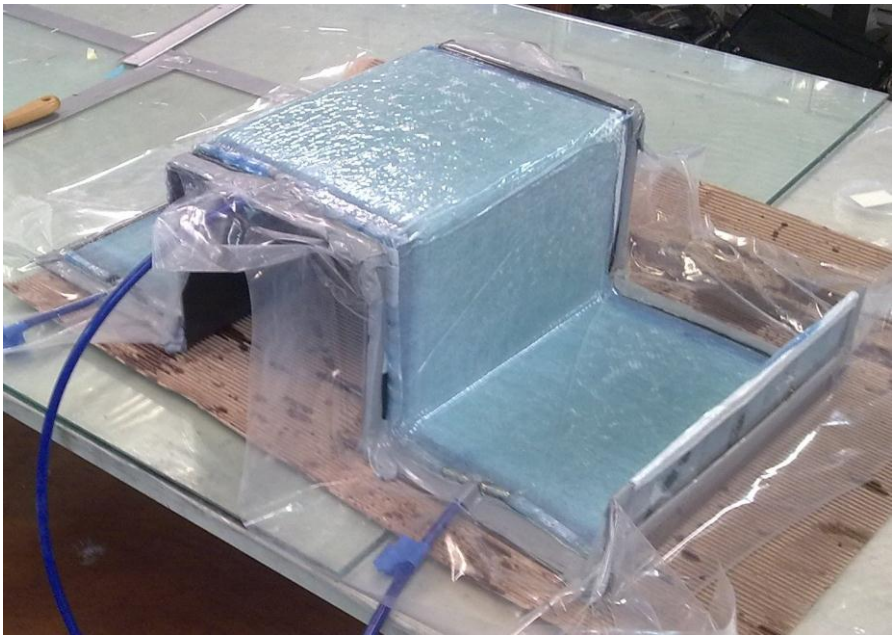

Figure 4.17: Vacuum bagging construction.

4.3.2 Specimens manufacturing

Preparation had to be done before the construction of the laminates on the tool could start. A thorough and comprehensive preparation would allow the construction process to run smoothly.

The tool had to be cleaned with acetone to remove oil residue from the steel press and dirt. Then, before each construction a special wax had to be applied on the tool's surface as a release agent which would allow the structure to be separated from the tool after the curing of the resin. In the vacuum construction cases ("C" &"D") it was very important to apply the sealant tape before the wax, in order to achieve a strong adhesion of the sealant tape. Also masking had to be done in the places where the vacuum hoses would be secured.

The fabrics for all the constructions were cut in advance. The dimensions were 1190 mm x 300 mm, with the warp direction of the fabric parallel to the large side. By using these dimensions there would be enough space left on the tool around the laminate for the sealant tape of the vacuum construction. The films and fabrics necessary for the vacuum bagging construction were also cut using the glass fabrics as a guide. It was important that the peelply would be larger than the glass fabric and that the perforated film would fully overlap it. Furthermore, the breather should be smaller than the perforated film so that would separate easier once the resin had cured but still fully overlap the glass fabric. Additionally,

before every construction, each ply was positioned on the tool without resin in the same order that would appear on the laminate and trimming was done where necessary.

Moreover, for the vacuum cases the spiral and the vacuum tubes had to be prepared. Because of the complex shape of the tool the spiral tube had to be pre-stretched and shaped to match the corners of the tool. This was achieved with the use of an industrial grade hot air blow gun. Three vacuum tubes were connected to the spiral tube, one on the middle of each level (Figure 4.17). This layout was chosen so that a uniform vacuum and suction of the resin on all three levels was achieved.

For the epoxy constructions the resin had to be mixed with the hardener on a weight ratio of 2 to 1. In order to calculate the mass of the resin required, the fabrics were weighted first and their mass was increased by 20%. This value was used for the mass of the resin needed. Since the ideal resin to fabric weight ratio was 1 to 1, the extra 20% was added to cover for losses of the resin on the mixing containers and construction tools. The gel time of this particular resin was 40 minutes. This was enough time for the HLU construction where only four plies of fabric were used. In the vacuum bagging construction however, more time was needed because there were six plies of fabric plus the layers of materials for the vacuum bagging. This problem was solved by dividing the resin and the hardener in two parts each and mixing the second part only after the first four plies of the construction were laid down on the tool.

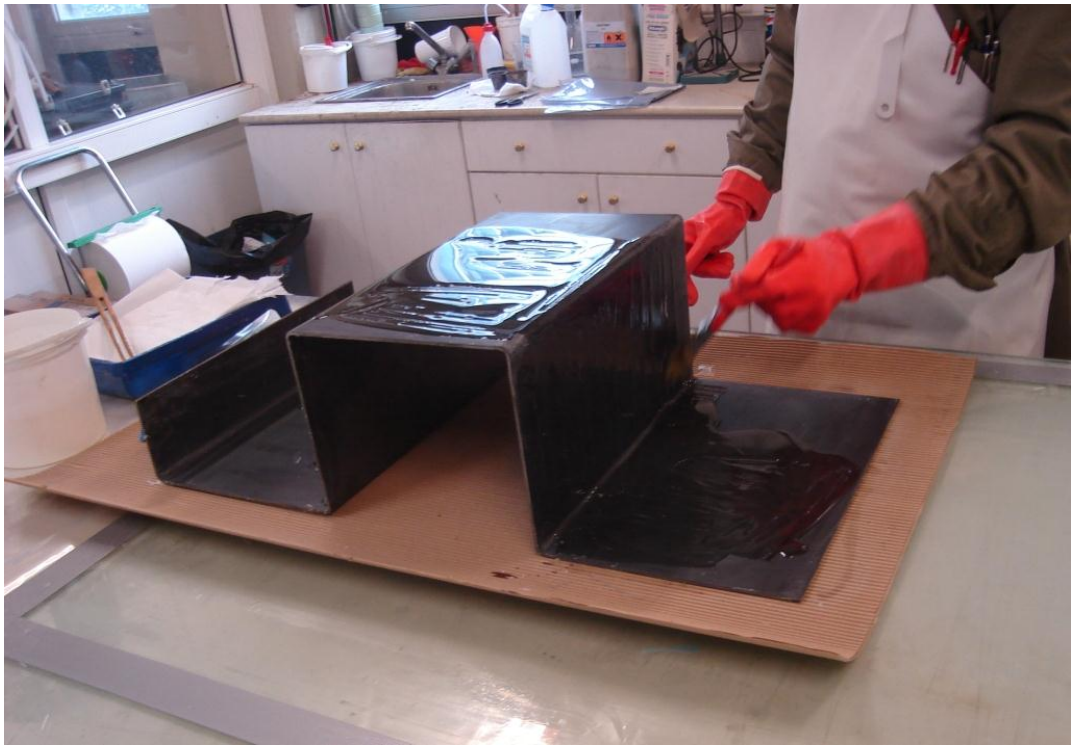

Figure 4.18: Using a brush to spread the resin on the tool.

For the polyester construction, the resin had to be mixed with the catalyst, where the catalyst's mass was 1.2% of the weight of the resin. This resin had a gel time of 18 minutes which was not enough to complete the construction. Because of that the resin and the hardener had to be split in two parts, with the second part mixed only after the first two layers of the structure were laid down on the tool. It should be noted that in the polyester

construction the use of breathing masks was necessary in order to prevent the persons involved from inhaling hazardous styrene fumes emitted from the resin.

The first step of the construction was to pour a part of the mixed resin on the tool and use a brush to spread it evenly on its surface (Figure 4.18). Then the first layer of fabric was pressed on its position by using a metal roll to force it to soak on the resin. Next, more resin was added on top and the process was repeated for the next layer. As mentioned before, the first half of the layers were positioned with the chopped strand mat facing downwards and the other half with the chopped strand mat facing upwards, so that the structure would be symmetrical. During the construction the persons involved wore plastic gloves and aprons so that their skin would not get in touch with the resin.

At the vacuum bagging cases, after all the layers of the glass fabric were in place, four more layers of fabrics and plastic films had to be added which were necessary for the vacuum. The first one was the peelply (Figure 4.19) [22]. This layer allows the resin to flow through it and its function is to make it possible for the next layer which is the perforated film

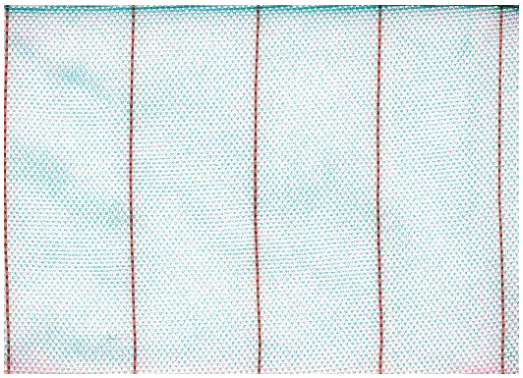

Figure 4.19: Peelply fabric [22].

Figure 4.20: Perforated film [22].

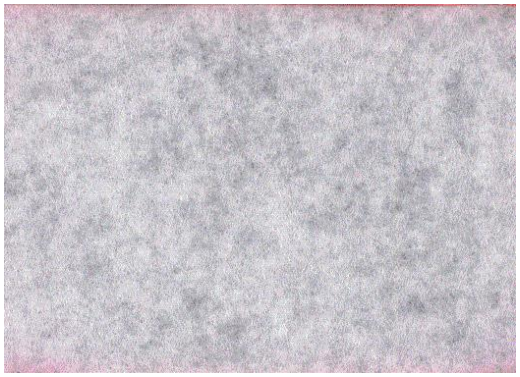

Figure 4.21: Breather fabric [22].

Figure 4.22: Vacuum film [22].

(Figure 4.20) [22], to separate from the composite structure when the resin has cured. The perforated film allows the next layer, which is the breather (Figure 4.21) [22] to separate from the peelply thus facilitating their removal from the structure after the resin is cured. It is also permeable by the resin. The breather's function is to soak on the excess of the resin which is forced out from the structure when the vacuum is applied. Before the last layer could be applied, the spiral tube which was already connected to the vacuum pipes was put in place. Extra sealant tape was used in the places where the vacuum tubes met with the sealant tape to ensure there would be no leaks after the vacuum film (Figure 4.22) [22] was applied. Then,

and only after the masking from the sealant tape was removed, the vacuum film was put in place. The vacuum film's function is to seal the construction so that vacuum can be applied.

The next step on the vacuum cases was to activate the vacuum pump. The vacuum level was set at 80%. When the vacuum level started to rise the construction was inspected closely for leaks. The leaks could be easily detected by listening since they created a distinctive sound. After they were spotted they were sealed with extra sealant tape. Then the pump was switched off and the vacuum gauge was checked periodically to verify that the vacuum level remained fixed at 80%.

After the curing was over, 24 hours past the construction, removing the structure from the tool was the next step. This was easily done in the HLU cases where a metal scraper was used to push the structure away from the tool. However, this was not the case for the vacuum bagging constructions. All the film layers that were used for the vacuum had to be removed before being able to separate the structure from the tool. Firstly, the vacuum film which was glued in one piece together with the breather fabric and the perforated film were removed by pulling the part of the film that was outside the sealant tape away from the structure (Figure 4.23). The peelply was removed likewise but required a greater amount of force to separate it from the structure. Then the structure was removed from the tool as in the HLU cases.

Figure 4.23: Removal of the vacuum film.

For cases "B" and "D" post curing was performed. The post curing furnace was pre-heated at 100 ^{o}C and the structure together with the tool was put inside. They were left there for two hours and then removed and left to cool down in a room where the temperature was set at 25 ^{o}C.

The last steps before the drilling were the trimming of the edges of the structures, as well as the measurement of the thickness of each structure. The edges of composite structures that are either by HLU or by the vacuum bagging method are always more or less uneven.

This happens because during the construction process, the different layers of the glass fabrics cannot always overlap perfectly. The trimming was done in order to better define the edges of the structure and to cut out the thin edges where the thickness was significantly smaller than the rest of the structure. The trimming was done by the use of a handheld reciprocating saw. The trimming of the edges also allowed for a more accurate thickness measurement using a digital calliper. The thickness was measured on various parts of each laminate and the average value was calculated. The thickness was on average higher at levels “B” and “C” and lower at level “A”, presenting a higher variation on the HLU structures than on the vacuum construction structures. This process was necessary in order to define the increment depth for the hole drilling.

4.3.3 Hole drilling

The number and the position of the holes had to be determined before the experiments could start. Firstly, it was decided that there should be three holes on level “A” and two holes on levels “B” and “C” drilled from the smooth side of the laminate (the one in contact with the tool). All these holes were positioned on the same line, across the longitudinal axis of the structure. On each level a uniform residual stress distribution was assumed through the length of the level, so it was expected that the measurements would be similar, since the holes were in the same line and had enough distance from the edges and the corners of the structure. So, the purpose of drilling more than one hole on each level was to verify that the values of the measurements were repeated. However, this assumption was not verified on

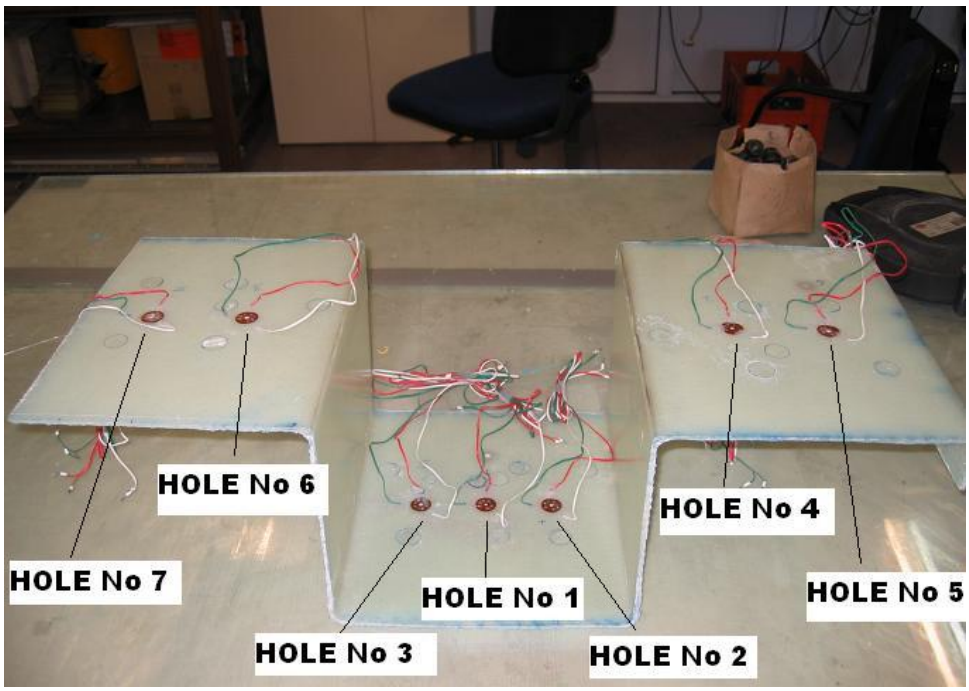

Figure 4.24: Holes drilled on the tool side (smooth side) of the composite structures.

the laminates that were drilled first (cases “A”, “C” and “D”) and then it was decided that only three holes would be drilled on the smooth side of the laminates in cases “B” and “E”, one hole on each level. Instead of drilling more holes on the smooth side of these laminates, two holes were drilled on the rough side of all the structures.

The holes should be far enough apart so that by drilling one, the residual stress field on the next one would not be affected. Since no information was found in literature on how far apart from each other the holes should be drilled, a distance of 80 mm was considered safe,

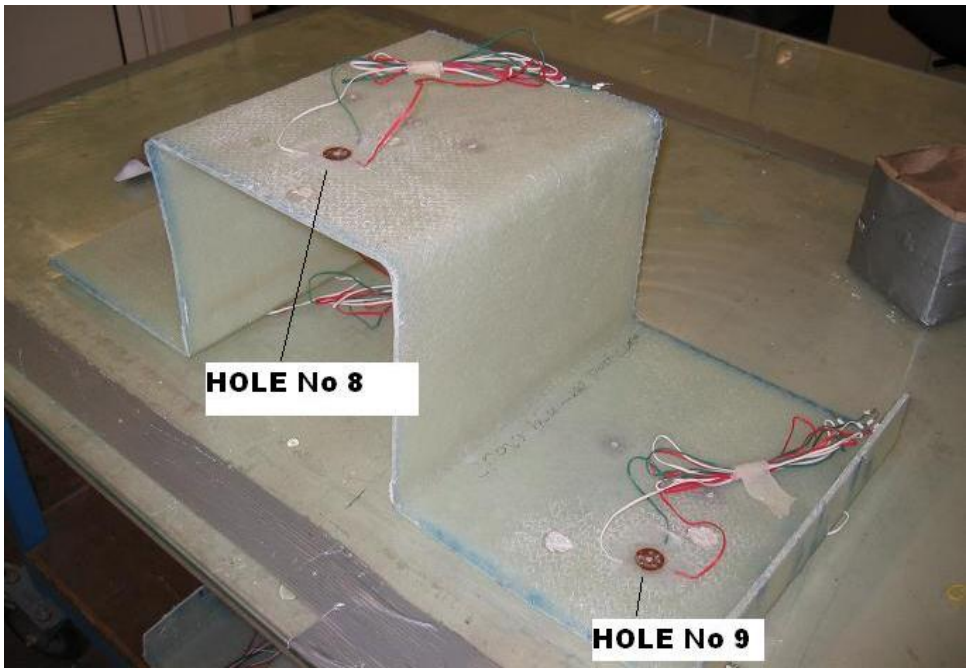

Figure 4.25: Holes drilled on the rough side of the composite structure.

taking into consideration the outer gauge diameter of 20 mm and also the available space on every level of the structure. They should also have enough distance from the corners of the structure so that there would be enough space for the hole drilling equipment to be attached. In all the levels the holes were equally distanced from each other and from the angles of the structure. On the rough side the holes were positioned 50 mm away in the transverse direction from the holes of the smooth side on the transverse axis of the structure. The numbers corresponding to the holes in Figures 4.24 and 4.25 represent the drilling sequence. The position of the holes on the structure is illustrated in Figures 4.24 and 4.25 which show the smooth side and the rough side of the structure, respectively.

Before bonding the strain gauges, the surface of the structure was properly prepared. Firstly, longitudinal and transverse lines were carved to mark the centre of each hole. These lines had to be aligned with the guide marks on the strain gauge rosettes so that two of the gauges of the rosette would measure the strains on the main directions of the structure which coincided with the warp and fill directions of the fibres, while the third one would measure the strains at an angle of 45^{o} from the other two. The surface was then thoroughly cleaned using an acetone solution. This allowed the rosettes to be glued firmly in place using cyanoacrylate glue. The wires attached to the rosettes were secured with a tape which would keep them in place until the drilling of the hole. On the rough side one more step had to be taken. Before the marking, the area where the rosette was to be glued was lightly sanded down with sandpaper to even it out. The sanding was as little as possible so as not to alter the residual stresses field around the hole area.

The next step was the attachment of the hole drilling apparatus (Figure 4.26). The area around the rosette was first cleaned using an acetone solution and then was marked around the three legs of the hole drilling apparatus. This was done by using a special stencil and a

marker. Cyanoacrylate glue was applied on the marked spots and the equipment was put in place. Since this glue only needed a few seconds to cure, pressure was applied on the equipment for only about thirty seconds and then it was left undisturbed for about fifteen minutes.

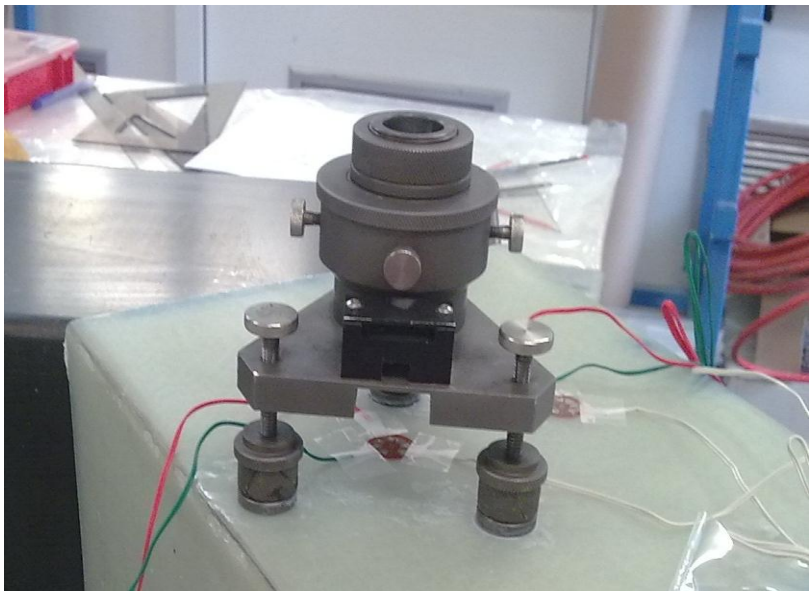

Figure 4.26: The hole drilling apparatus attached on the smooth side of the composite structure.

The calibration of the hole drilling equipment was the next step. The device was adjusted properly so that the hole was drilled perpendicularly to the structure. The depth probe of a vernier calliper was used to measure the distance between the device and the structure. Adjustments were made until this distance was the same all around the device. In order to get accurate measurements, drilling in the exact centre of the rosette was very important. A special scope was fitted in the device instead of the drill and was adjusted until the focus was clear. Then, the scope was moved using the calibrating screws until it aimed at the centre of the rosette. Afterwards, the screws were tightened and the scope was removed. Finally the vernier device which is illustrated in Figure 4.27 was put in place. The function of this device was to adjust the increment depth at steps of 0.02 mm. This device came with a holding ring which was necessary to prevent the device from rotating during drilling.

The next step was to prepare the drill. The drill bit was attached at one end of a circular section bar. This bar was designed to just fit in the hole at the centre of the base of the hole drilling equipment. Near the top of the round bar a metal ring (shown in Figure 4.28) was tightened in place. This metal ring limited the hole depth to what was dictated by the vernier device. Between this ring and the vernier device a flat aluminium washer was positioned in order to protect the face of the vernier device from friction-induced wear. The position of this ring had to be adjusted before the drilling could start. This was done by inserting the bar until the drill bit touched the rosette and then secure the metal ring with its face touching the washer on top of the vernier device. It should be noted that before securing this ring, the vernier's reading was set to zero.

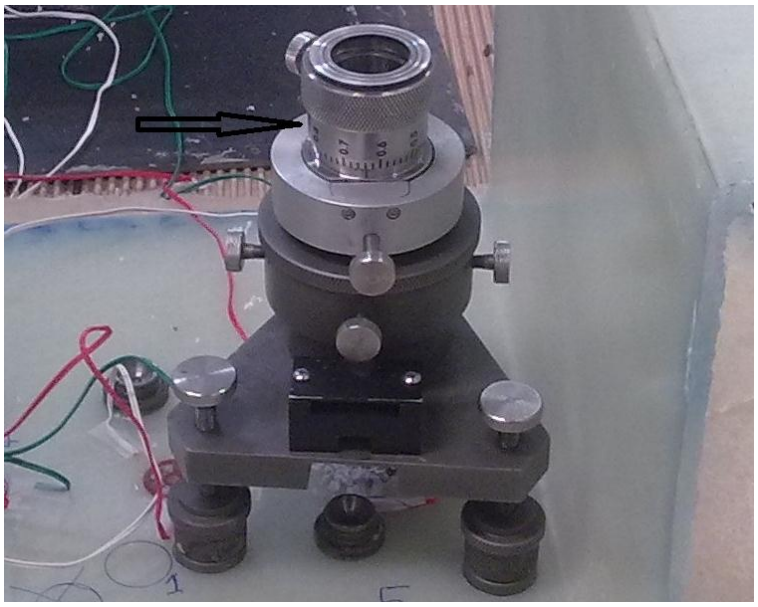

Figure 4.27: The vernier device (illustrated) placed on the hole drilling apparatus secured with its holding ring.

The last step before the drilling could start was to connect the wires attached to the strain gauges of the rosette to a data acquisition device that displayed the strain readings. The structure was then put in place for drilling.

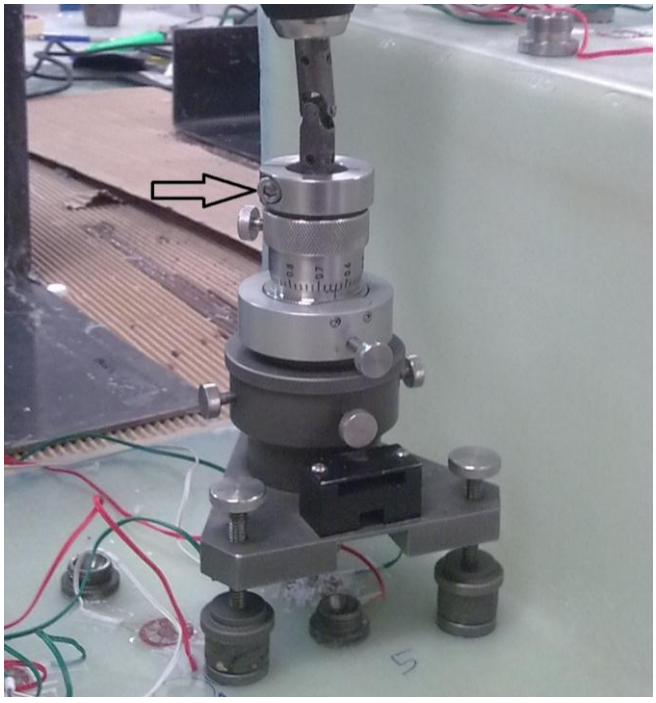

Figure 4.28: The hole-drilling equipment with the drill positioned in place for drilling. The metal ring (illustrated) is tightened in place.

The incremental depth was first calculated by dividing the already measured structure's thickness by the number of increments. Drilling with two increments per ply was decided since it was both accurate, as proven in reference [18], and time efficient. Therefore, the number of increments was 8 for the HLU structures and 12 for the vacuum bagging

structures. The electric drill was positioned in place and maximum rpm were achieved before the drill bit touched the rosette. The hole was then drilled by applying only a very slight force on the electric drill and the drill was stopped and removed from the equipment. The readings were written down when they settled, which happened just after a few seconds. The vernier was then set to the next increment depth and the process was repeated until all the increments were drilled. Because the thickness of the structure was larger than the range of the vernier, it required to be set to zero half way through the hole and the drill to be readjusted. The results of the measurements are presented in tables 5.1 through 5.5 in the following chapter.

After the drilling of the hole was over, the equipment was removed. This was done by unscrewing the parts that were glued to the structure from the device. These parts were left attached to the structure (see Figures 4.27 and 4.28) while others were used for the drilling of next hole. Their removal was performed only after all the holes on each level they were drilled. This way, the damage done to the structure during their removal could not affect the measurements on the adjacent holes.

5. EXPERIMENTAL RESULTS

In the following tables the strain measurements from the hole drilling experiments for each case are presented. The unit for the measurements is microstrain (με). The position of the holes on the structure according to their corresponding numbers is shown in Figures 4.24 and 4.25. The 0°, 90°, 45° indications under each hole number refer to the orientation of the three different gauges on each rosette. Furthermore, the increment number is indicated by the first number on each row. In the cells where "-" is presented no measurements were taken.

Table 5.1: Strains measured in Case "A" (epoxy resin with Agimat WRM-600.300 glass fibres, hand lay up, cold cured).

		Hole No 1			Hole No 2			Hole No 3		
		0º	90º	45º	0º	90º	45º	0º	90º	45º
Increment No	1	17	29	20	-37	44	6	17	26	0
	2	3	44	17	-45	58	14	6	32	-3
	3	-6	46	17	-54	52	11	-6	32	-6
	4	-11	32	14	-59	46	6	-11	39	-6
	5	-8	32	14	-65	46	3	-8	26	-3
	6	-14	32	11	-68	44	3	-11	20	-6
	7	-6	32	17	-65	44	3	-3	23	6
	8	-6	32	14	-71	44	-6	-3	26	3
		Hole No 4			Hole No 5			Hole No 6		
		0º	90º	45º	0º	90º	45º	0º	90º	45º
Increment No	1	3	3	23	31	26	49	-3	9	29
	2	-17	-12	11	39	29	63	8	-20	26
	3	-34	-20	11	42	32	66	8	-23	29
	4	-48	-26	0	37	29	63	-3	-38	26
	5	-62	-32	-9	34	26	69	-6	-38	26
	6	-71	-35	-9	34	29	69	-3	-32	29
	7	-79	-26	-9	34	35	69	17	-35	43
	8	-79	-26	-9	28	29	69	37	-12	69
		Hole No 7			Hole No 8			Hole No 9		
		0º	90º	45º	0º	90º	45º	0º	90º	45º
Increment No	1	45	32	31	6	-3	11	-14	-20	-14
	2	51	35	40	-11	-6	9	-11	-20	-14
	3	56	38	51	-20	-9	11	-11	-20	-17
	4	54	32	49	-25	-15	11	-8	-17	-26
	5	51	29	54	-28	-17	11	-3	-9	-11
	6	51	23	60	-31	-20	11	-3	-6	-3
	7	48	17	60	-31	-35	9	-11	-15	-9
	8	37	12	51	-34	-35	9	-11	-15	-9

Table 5.2: Strains measured in Case "B" (epoxy resin with Agimat WRM-600.300 glass fibres, hand lay up, post cured).

		Hole No 1			Hole No 2			Hole No 3		
		0°	90°	45°	0°	90°	45°	0°	90°	45°
Increment No	1	11	15	26	-	-	-	-	-	-
	2	8	12	37	-	-	-	-	-	-
	3	6	6	29	-	-	-	-	-	-
	4	3	3	29	-	-	-	-	-	-
	5	-3	-9	26	-	-	-	-	-	-
	6	-6	-12	20	-	-	-	-	-	-
	7	-23	-29	6	-	-	-	-	-	-
	8	-17	-26	9	-	-	-	-	-	-
		Hole No 4			Hole No 5			Hole No 6		
		0°	90°	45°	0°	90°	45°	0°	90°	45°
Increment No	1	-	-	-	23	29	26	-	-	-
	2	-	-	-	31	32	34	-	-	-
	3	-	-	-	28	29	31	-	-	-
	4	-	-	-	25	26	31	-	-	-
	5	-	-	-	25	23	26	-	-	-
	6	-	-	-	28	26	26	-	-	-
	7	-	-	-	25	20	23	-	-	-
	8	-	-	-	31	26	26	-	-	-
		Hole No 7			Hole No 8			Hole No 9		
		0°	90°	45°	0°	90°	45°	0°	90°	45°
Increment No	1	23	-3	23	14	17	17	6	12	6
	2	25	-3	29	45	26	34	14	17	6
	3	23	-3	26	54	23	37	8	9	9
	4	20	-9	23	56	9	29	3	6	6
	5	11	-12	17	42	12	34	-8	-3	3
	6	11	-15	17	45	12	34	-20	-12	-3
	7	11	-23	14	65	-26	29	-28	-29	-9
	8	8	-23	14	48	-12	31	-28	-32	-6

Table 5.3: Strains measured in Case "C" (epoxy resin with Agimat WRM-600.300 glass fibres, vacuum bagging, cold cured).

		Hole No 1			Hole No 2			Hole No 3		
		0º	90º	45º	0º	90º	45º	0º	90º	45º
Increment No	1	-6	-32	3	-23	3	-9	-14	-12	-6
	2	-11	-35	0	-34	9	-11	-20	-20	-9
	3	-14	-29	3	-42	6	-14	-23	-26	-14
	4	-14	-23	6	-48	3	-23	-34	-32	-20
	5	-17	-23	3	-51	0	-26	-37	-35	-20
	6	-17	-20	6	-54	-9	-29	-42	-41	-26
	7	-14	-17	9	-59	-38	-31	-48	-44	-29
	8	-17	-15	9	-59	-44	-31	-51	-44	-34
	9	-17	-15	11	-62	-52	-34	-54	-46	-37
	10	-17	-15	23	-59	-55	-31	-48	-38	-31
	11	-17	-12	20	-59	-55	-34	-59	-46	-40
	12	-17	-12	20	-62	-55	-37	-62	-46	-40
		Hole No 4			Hole No 5			Hole No 6		
		0º	90º	45º	0º	90º	45º	0º	90º	45º
Increment No	1	-37	-12	0	-87	9	-6	14	-9	6
	2	-39	-26	-20	-113	9	-6	23	-3	9
	3	-51	-26	-23	-127	6	-9	25	-23	6
	4	-45	-20	-20	-135	-6	-9	28	-9	11
	5	-45	-20	-17	-141	-6	-9	28	-15	11
	6	-48	-20	-23	-147	-9	-9	28	-17	9
	7	-39	-15	-14	-150	-9	-11	25	-20	9
	8	-37	-12	-14	-152	-9	-11	25	-23	6
	9	-37	-9	-14	-155	-9	-11	25	-23	9
	10	-34	-3	-11	-155	-9	-9	28	-26	14
	11	-31	-3	-9	-161	-6	-11	28	-26	14
	12	-28	0	-6	-161	-6	-11	31	-26	14
		Hole No 7			Hole No 8			Hole No 9		
		0º	90º	45º	0º	90º	45º	0º	90º	45º
Increment No	1	6	-3	0	-31	-6	-9	0	0	3
	2	11	-20	-9	-34	-20	-6	-3	12	14
	3	14	-23	-9	-23	-20	6	-3	12	14
	4	14	-9	-11	-34	-32	-3	-8	6	14
	5	11	-15	-9	-37	-32	3	-11	3	14
	6	14	-17	-3	-37	-38	6	-11	-12	17
	7	8	-20	-9	-39	-38	3	-14	-15	14
	8	8	-23	-6	-39	-41	3	-17	-17	14
	9	8	-23	-9	-39	-41	3	-25	-26	14
	10	8	-26	-11	-39	-41	6	-31	-32	9
	11	3	-26	-11	-37	-38	9	-28	-32	11
	12	8	-26	-11	-34	-38	11	-28	-32	11

Table 5.4: Strains measured in Case "D" (epoxy resin with Agimat WRM-600.300 glass fibres, vacuum bagging, post cured).

		Hole No 1			Hole No 2			Hole No 3		
		0º	90º	45º	0º	90º	45º	0º	90º	45º
Increment No	1	-23	-9	-6	-14	-3	3	-3	6	9
	2	-34	-12	-17	-17	-3	6	-11	0	11
	3	-39	-17	-17	-17	-3	9	-20	0	9
	4	-45	-20	-23	-20	-9	9	-25	0	9
	5	-51	-26	-29	-23	-12	9	-31	-3	11
	6	-56	-35	-37	-34	-15	6	-37	-6	9
	7	-59	-35	-40	-42	-26	-3	-45	-12	9
	8	-62	-38	-43	-45	-32	-3	-51	-15	9
	9	-62	-41	-49	-51	-35	-6	-59	-20	6
	10	-68	-44	-54	-54	-38	-9	-62	-26	0
	11	-71	-46	-60	-56	-44	-11	-71	-32	-6
	12	-71	-49	-60	-59	-44	-14	-71	-32	-6

		Hole No 4			Hole No 5			Hole No 6		
		0º	90º	45º	0º	90º	45º	0º	90º	45º
Increment No	1	8	3	9	17	-6	17	3	3	6
	2	6	17	14	20	-6	23	8	6	11
	3	0	15	20	20	-9	26	3	12	17
	4	-3	9	20	14	-17	29	-6	3	14
	5	-3	9	20	8	-20	29	-8	3	14
	6	-8	3	17	8	-26	29	-14	-9	9
	7	-11	0	14	8	-29	26	-23	-12	3
	8	-17	-3	11	6	-32	2	-25	-15	0
	9	-17	-6	9	3	-35	20	-28	-17	-6
	10	-20	-12	6	0	-41	23	-34	-26	-9
	11	-25	-15	6	0	-41	17	-42	-32	-14
	12	-23	-12	6	3	-38	23	-42	-29	-11

		Hole No 7			Hole No 8			Hole No 9		
		0º	90º	45º	0º	90º	45º	0º	90º	45º
Increment No	1	8	23	9	6	0	14	-3	12	6
	2	14	20	11	48	6	40	3	12	6
	3	6	15	6	56	0	43	3	15	9
	4	3	12	6	56	3	46	-6	9	9
	5	0	3	3	56	0	54	-11	9	9
	6	-3	0	0	56	-3	51	-11	6	9
	7	-8	-6	-6	56	-3	57	-11	3	6
	8	-8	-6	-6	62	-6	63	-11	0	6
	9	-14	-11	-11	59	-9	63	-14	-6	3
	10	-14	-9	-9	59	-15	60	-25	-15	-3
	11	-17	-11	-11	56	-20	60	-28	-17	-3
	12	-17	-14	-14	56	-15	63	-25	-15	-3

Table 5.5: Strains measured in Case “E” (polyester resin with Agimat WRM-600.300 glass fibres, hand lay up, cold cured)

		Hole No 1			Hole No 2			Hole No 3		
		0º	90º	45º	0º	90º	45º	0º	90º	45º
Increment No	1	-8	15	3	-	-	-	-	-	-
	2	-8	29	9	-	-	-	-	-	-
	3	-11	23	11	-	-	-	-	-	-
	4	-11	20	14	-	-	-	-	-	-
	5	-14	17	14	-	-	-	-	-	-
	6	-17	17	17	-	-	-	-	-	-
	7	-20	15	14	-	-	-	-	-	-
	8	-23	9	9	-	-	-	-	-	-
		Hole No 4			Hole No 5			Hole No 6		
		0º	90º	45º	0º	90º	45º	0º	90º	45º
Increment No	1	-	-	-	-42	-6	3	-	-	-
	2	-	-	-	-39	-6	11	-	-	-
	3	-	-	-	-45	-12	14	-	-	-
	4	-	-	-	-54	-17	9	-	-	-
	5	-	-	-	-56	-20	9	-	-	-
	6	-	-	-	-59	-26	6	-	-	-
	7	-	-	-	-65	-29	-3	-	-	-
	8	-	-	-	-65	-26	-9	-	-	-
		Hole No 7			Hole No 8			Hole No 9		
		0º	90º	45º	0º	90º	45º	0º	90º	45º
Increment No	1	-14	-6	14	0	9	0	96	12	54
	2	-14	-6	14	-6	9	11	110	32	80
	3	-23	-12	14	8	3	11	113	35	83
	4	-25	-17	11	20	0	17	113	38	86
	5	-28	-20	9	20	6	17	121	32	86
	6	-34	-26	6	31	-3	11	118	26	83
	7	-37	-29	0	17	-17	3	121	29	77
	8	-34	-32	3	14	-26	-9	102	-15	49

6. CONCLUSIONS

The results from the measurements taken were studied in order to verify whether or not variations in structural methods and tool-imposed restrictions affect the level of the residual stresses present in a composite structure. All the measurements were checked for consistency and repeatability through thorough comparison that occurred in several stages.

Initially, the values measured for the different holes of each level were compared to each other (cases “A”, “C” and “D” where more than one hole per level were drilled on the smooth side of the structure), in order to verify the repeatability of the measurements. During this stage of the comparison no consistency or repeatability in the results could be observed. In case “A” for example, it is clearly visible in Table 5.1 that no common trends exist between the measurements of the holes 1, 2 and 3 which are on the same level. More specifically, the minimum value observed in hole No 1 is -14 με while in hole No 2 is -71 με. During this stage of the comparison no consistency or repeatability in the results could be observed.

The second step was the comparison between the readings for the different directions of the strain gauges on each rosette. By doing so, it was possible to spot possible common trends that would verify whether or not a difference in the level of the residual stresses between the different directions exists. A higher level of residual stresses was expected in the 0° direction due to the geometrical restrictions of the tool. This assumption however was not verified by the measurements. It can be seen for example in case “A” (Table 5.1) that holes No 1 and No 3 present greater (absolute) values in the 90° direction whereas holes No 2 and No 4 presented greater values in the 0° direction and holes No 4 and No 5 in the 45° direction. Similar observations can be made in the other cases as well. Therefore, it is safe to say that no consistency or repeatability in the results could be observed during this stage of the comparison.

The comparison between the measurements in the different levels of the structures was done next. Higher levels of residual stresses were expected to be measured in level “A” (holes No 1, 2, 3 and 9) due to the geometrical restrictions of the tool. After studying the results it was obvious that this assumption was not confirmed.

In the next step the variation of the measurements was compared to their absolute values. In some occasions the variation was low compared to the range of the values as for example in case “B” hole No 5 (Table 5.2) in the 0° direction where the average value is 27 με and the range is 8 με which is about 30% of the average value. In other occasions however this was not the case. For example, in case “C” hole No 2 (Table 5.3) in the 90° direction where the absolute average value is 24 με and the range is 64 με which is about 2.66 times the average value.

The difference between the values of the holes drilled on the smooth side and the rough side of the composite was examined next. More specifically on level “A” the measurements of the holes No 1, 2 and 3 were compared to the measurements of hole No 8, while the measurements of the holes No 4 and 5 were compared to the measurements of hole No 9 on level “C”. By drilling holes on both sides of the structure it was possible to verify the through the thickness accuracy of the measurements. In order for the measurements to be accurate, the measurements corresponding to the hole drilled on the rough side should be a mirror image of the measurements of the holes drilled on the smooth side. After studying the results it was obvious that this was not the case since the above assumption was not verified.

The effects of post curing and manufacturing method were examined next. This was done by comparing the respective measurements between the cases “A” and “B”, and “C” and “D” (effect of post curing) and also between the cases “A” and “C”, and “B” and “D” (effect of manufacturing method). Finally, the readings for the polyester structure (case “E”) were examined in comparison to the other structures. In all the occasions the readings presented low values and so it was not possible to verify whether or not the level of the residual stress is affected by the post curing process or the difference between the manufacturing method and composite materials described above.

The goal of this study was to examine the residual stresses in typical marine structures and furthermore, to measure the effect of the tool shape, of the materials used and of the manufacturing method on the level of the residual stresses in such structures. After careful and thorough examination of the measurements, as described in the previous paragraphs, the results were not conclusive since the readings were generally low and presented no repeatability or consistency. The possible scenario for this outcome is that the level of the residual stresses in typical marine composites as the ones examined in this study is very low and therefore cannot be accurately measured using the incremental hole drilling method.

7. FUTURE WORK

In future work, a higher level or residual stresses could be induced in a composite structure in order to make the variance of the magnitude of the stresses in the different levels of the tool more distinct. This could be achieved by selecting different materials for the construction of the composite structure. In references [16], [18] and [19] the authors proved using the incremental hole drilling method that a high level of residual stresses exists in unidirectional prepreg carbon epoxy laminates. These materials may present a higher level of residual stresses but are not however commonly used in the shipbuilding industry.

Since this is still a field where research is still in the initial stages, some variations in the experimental method, i. e. a difference in drilling speed, hole diameter or strain-gage rosette type could produce different results. Furthermore, the use of a different experimental method (as described in chapter 3) could also produce different, possibly more accurate results.

Moreover, the level of the residual stresses on the structure is to be calculated by finite element analysis as described in chapter 3.5 of this study with the use of the measured strain values.

References

[1] Nicholas Tsouvalis, George Margelis, Dimitris Dellis, “Residual stresses in composite materials: a review”, NTUA Report No MAR-R4-3-NTUA-24(2) for MARSTRUCT, January 2009

[2] Göran Fernlund, Anoush Poursartip, Graham Twigg, Carolyne Albert, “Residual stress, spring-in and warpage in autoclaved composite parts”.

[3] Patricia P. Parlevliet, Harald E.N. Bersee, Adriaan Beukers, “Residual stresses in thermoplastic composites – A study of the literature – Part II: Experimenal techniques”, Composites: Part A 38 (2007) 651-665, © 2006 Elsevier Ltd.

[4] Graham Twigg, Anoush Poursartip, Göran Fernlund, “Tool-part interaction in composites processing. Part I: experimental investigation and analytical model”, Composites: Part A 35 (2004) 121-133, © 2004 Elsevier Ltd.

[5] M.A. Seif, U.A. Khashaba, R. Rojas-oviedo, “Residual stress measurements in CFRE and GFRE composite missile shells”, Composite Structures 79 (2007) 261-269, © 2006 Elsevier Ltd.

[6] M.A. Seif, S.R. Short, "Determination of residual stresses in thin-walled composite cylinders", Experimental Techniques, March/April 2002, 43-46.

[7] Tomasz Garstka, N. Ersoy, K.D. Potter, M.R. Wisnom, “In situ measurements of through-the-thickness strains during processing of AS4/8552 composite”, Composites: Part A 38 (2007) 2517-2526, © 2007 Elsevier Ltd.

[8] Patricia P. Parlevliet, Harald E.N. Bersee, Adriaan Beukers, “Residual stresses in thermoplastic composites – a study of the literature. Part III: Effects of thermal residual stresses”, Composites: Part A 38 (2007) 1581-1596, © 2007 Elsevier Ltd.

[9] D.D.L. Chung, “Thermal analysis of carbon fiber polymer-matrix composites by electrical resistance measurement”, Thermochimica Acta 364 (2000) 121-132, © 2000 Elsevier Science B.V.

[10] D. Karalekas, J. Cugnoni, J. Botsis, “Monitoring of process induced strains in a single fibre composite using FBG sensor: A methodological study”, Composites: Part A 39 (2008) 1118-1127, © 2008 Elsevier Ltd.

[11] M.G. Bateman, O.H. Miller, T.J. Palmer, C.E.P. Breen, E.J. Kingston, D.J. Smith, M.J. Pavier, “Measurement of residual stress in thick section composite laminates using the deep-hole method”, International Journal of Mechanical Sciences 47 (2005) 1718-1739, © 2005 Elsevier Ltd.

[12] Michael B. Prime, “Residual stress measurement by successive extension of a slot: The crack compliance method”, Los Alamos National Laboratory, Engineering Sciences and Applications Division, LA-UR-98-3857, Applied Mechanics Reviews, Vol. 52, No. 2, pp. 75-96, 1999.

[13] Gary S. Schajer, Michael B. Prime, “Use of inverse solutions for residual stress measurement”, January 2005, Los Alamos National Laboratory, Engineering Sciences and Applications Division, LA-UR-04-5890, Journal of Engineering Materials and Technology, Volume 128, Number 3, July 2006, 375-382.

[14] Michael B. Prime, “Experimental procedure for crack compliance (slitting) measurements of residual stress”, Los Alamos National Laboratory, Engineering Sciences and Applications Division, Prime, LA-UR-03-8629.

[15] Michael B. Prime, “Measuring residual stress and the resulting stress intensity factor in compact tension specimens”, Los Alamos National Laboratory, Engineering Sciences and Applications Division, LA-UR-98-782, Fatigue & Fracture of Engineering Materials & Structures, Volume 22, Number 3, March 1999, pp. 195-204.

[16] O. Sicot, X.L. Gong, A. Cherouat and J. Lu, "Determination of residual stress in composite laminates using the incremental hole-drilling method", Journal of Composite Materials, Vol. 37, No. 9/2003, © 2003 Sage Publications.

[17] R. Oettel, “The determination of uncertainties in residual stress measurement (using the hole drilling technique)”, Issue 1, September 2000, Manual of Codes of Practice for the determination of uncertainties in mechanical tests on metallic materials, Code of Practice No. 15, Standards Measurement & Testing Project No. SMT4-CT97-2165.

[18] O. Sicot, X.L. Gong, A. Cherouat, J. Lu, “Influence of experimental parameters on determination of residual stress using the incremental hole-drilling method”, Composites Science and Technology 64 (2004) 171-180, © 2003 Elsevier Ltd.

[19] A. Cherouat, X.L. Gong, O. Sicot, J. Lu, “Influence of the residual stresses on the mechanical behavior of advanced composite parts”, Journal of Neutron Research, 2001, Vol. 9, pp. 319-330

[20] A. Niku-Lari, J. Lu, J.F. Flavenot, “Measurement of residual-stress distribution by the incremental hole-drilling method”, Journal of Mechanical Working Technology, 11 (1985), pp. 167 – 188

[21] George Margelis, Konstantinos Stamatopoulos, Nicholas Tsouvalis, “Measurement of Residual Stresses in Typical Marine Composite Materials Using the Incremental Hole Drilling Method” NTUA Report No MAR-R4-3-NTUA-28(1) for MARSTRUCT, January 2010

[22] www.fibremax.eu website

Appendix A

Stress-strain diagrams

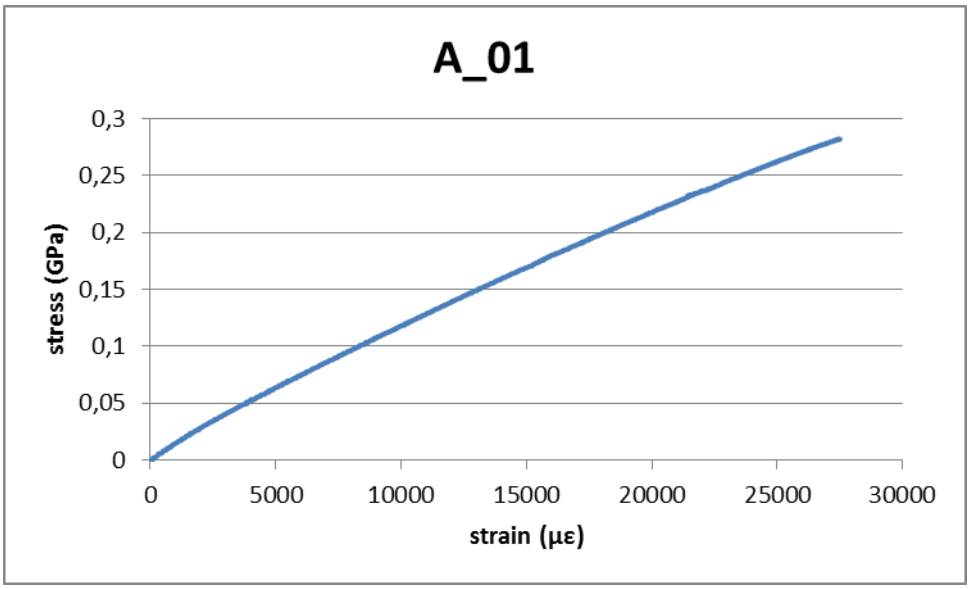

Figure A.1: Stress-strain diagram for specimen 1 of case “A” (Epoxy HLU-cold cured).

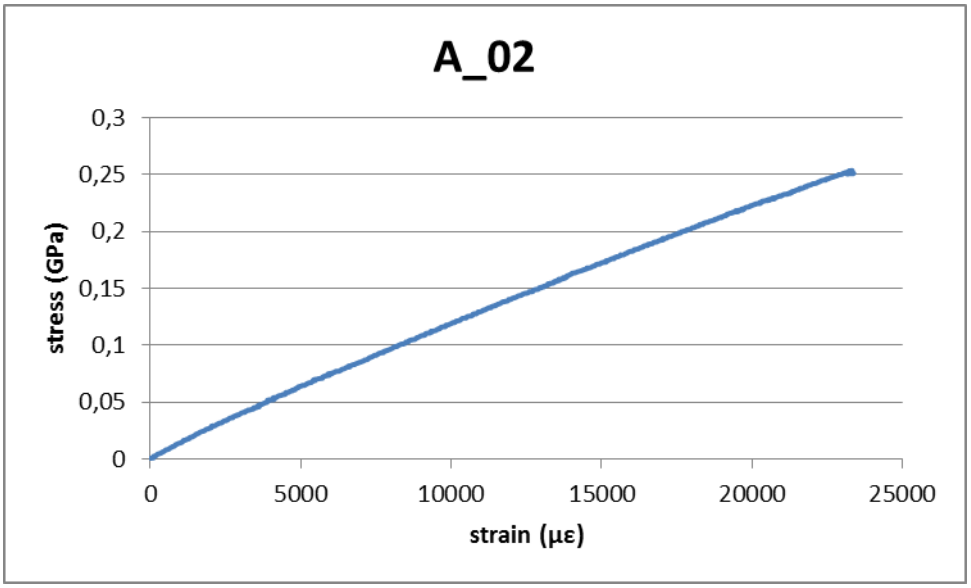

Figure A.2: Stress-strain diagram for specimen 2 of case “A” (Epoxy HLU-cold cured).

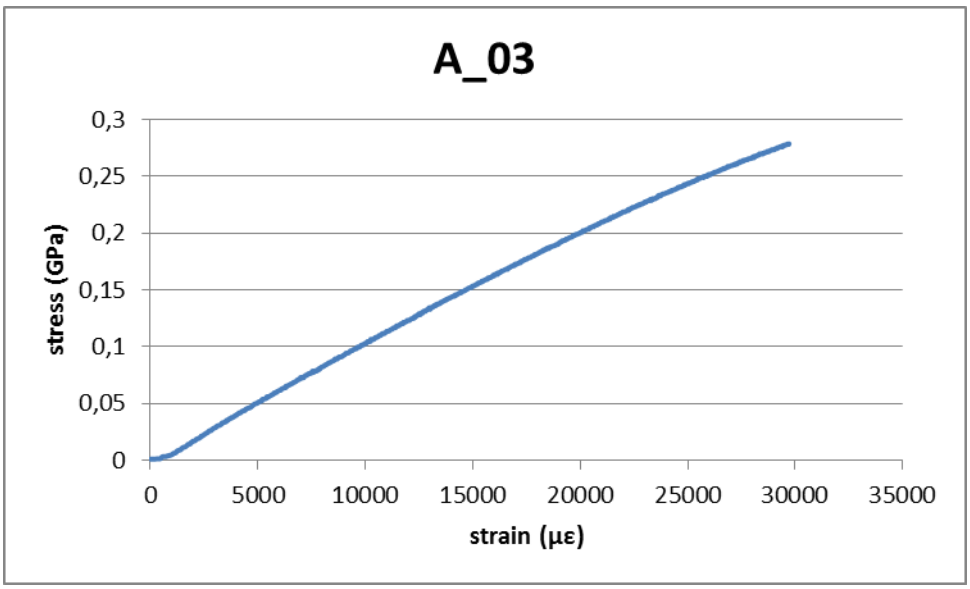

Figure A.3: Stress-strain diagram for specimen 3 of case “A” (Epoxy HLU-cold cured).

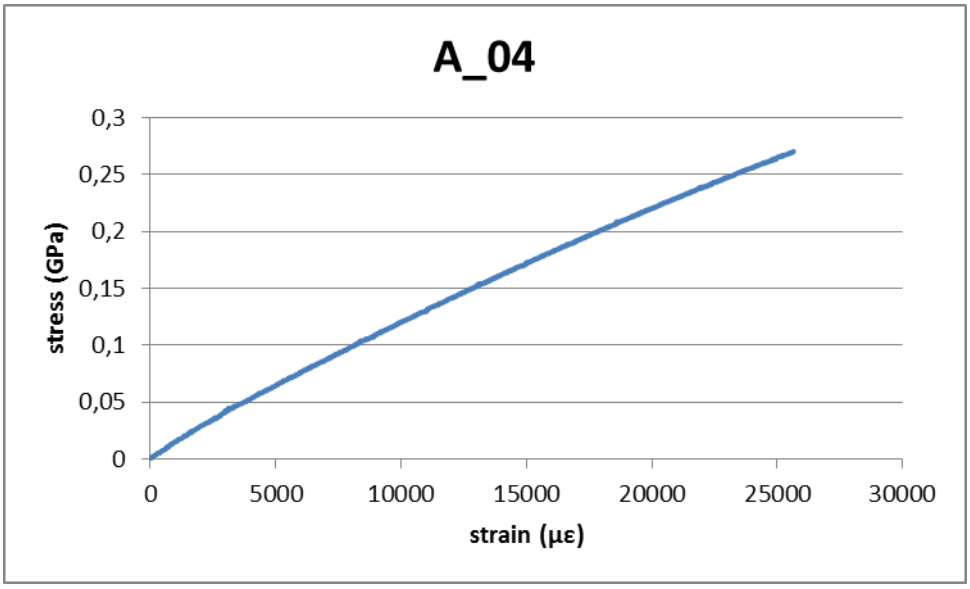

Figure A.4: Stress-strain diagram for specimen 4 of case “A” (Epoxy HLU-cold cured).

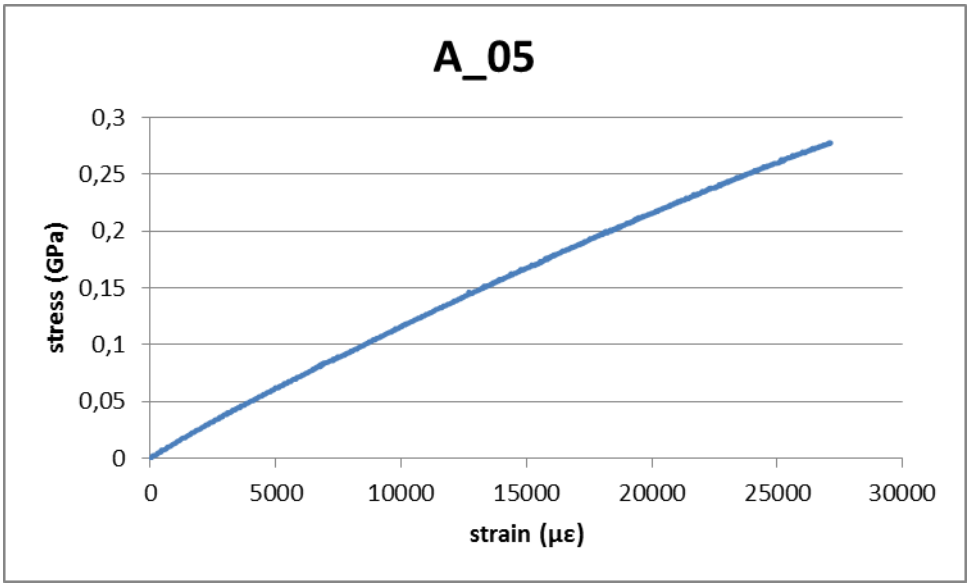

Figure A.5: Stress-strain diagram for specimen 5 of case “A” (Epoxy HLU-cold cured).

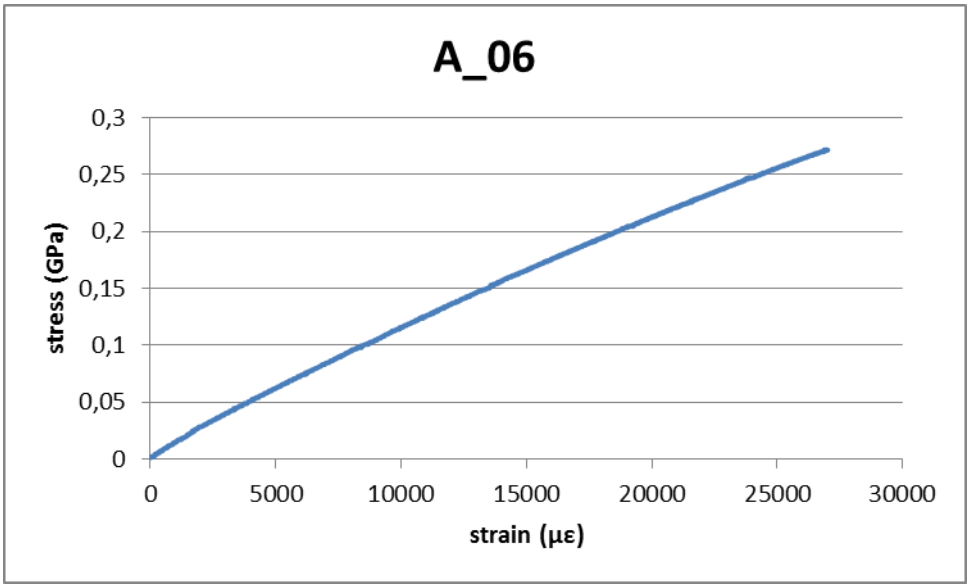

Figure A.6: Stress-strain diagram for specimen 6 of case “A” (Epoxy HLU-cold cured).

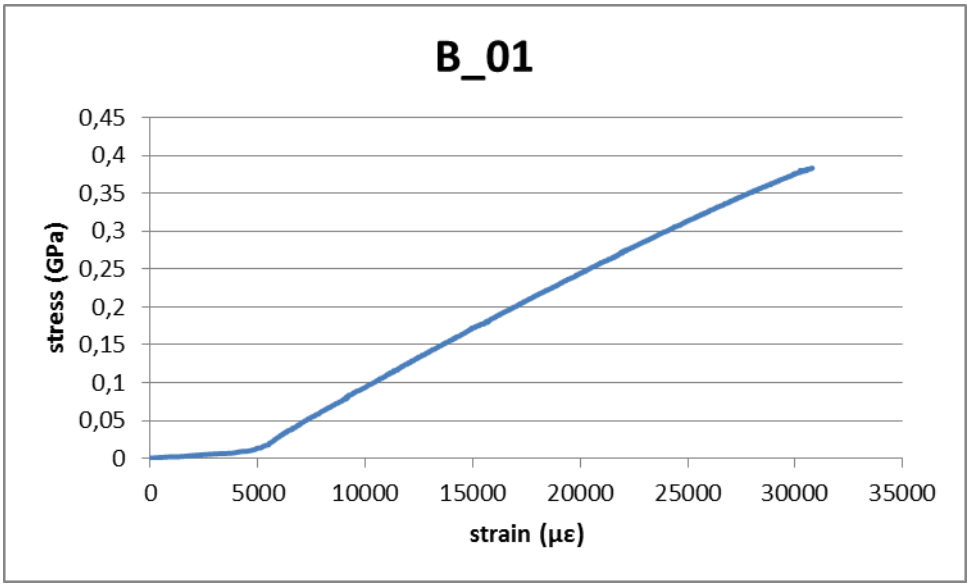

Figure A.7: Stress-strain diagram for specimen 1 of case “B” (Epoxy HLU-post cured).

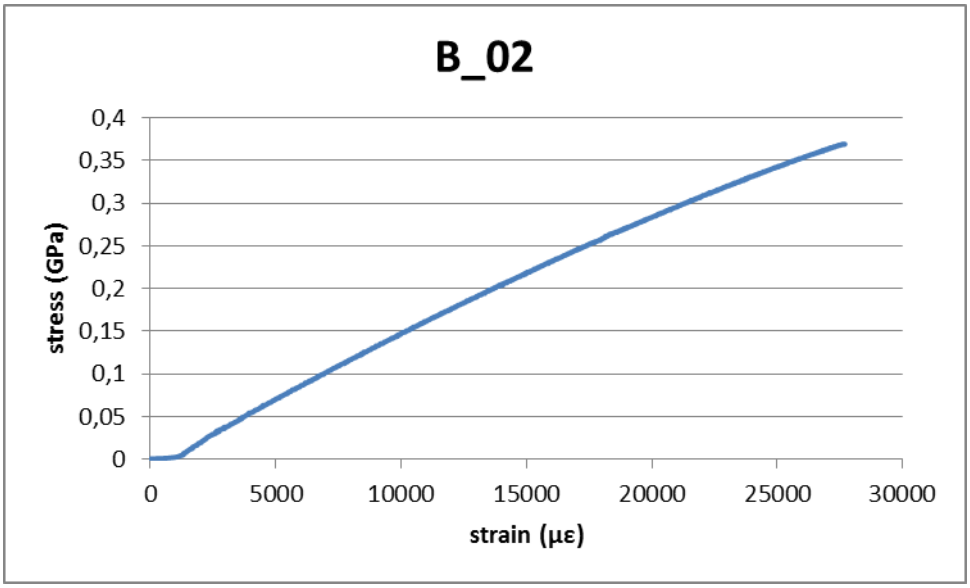

Figure A.8: Stress-strain diagram for specimen 2 of case “B” (Epoxy HLU-post cured).

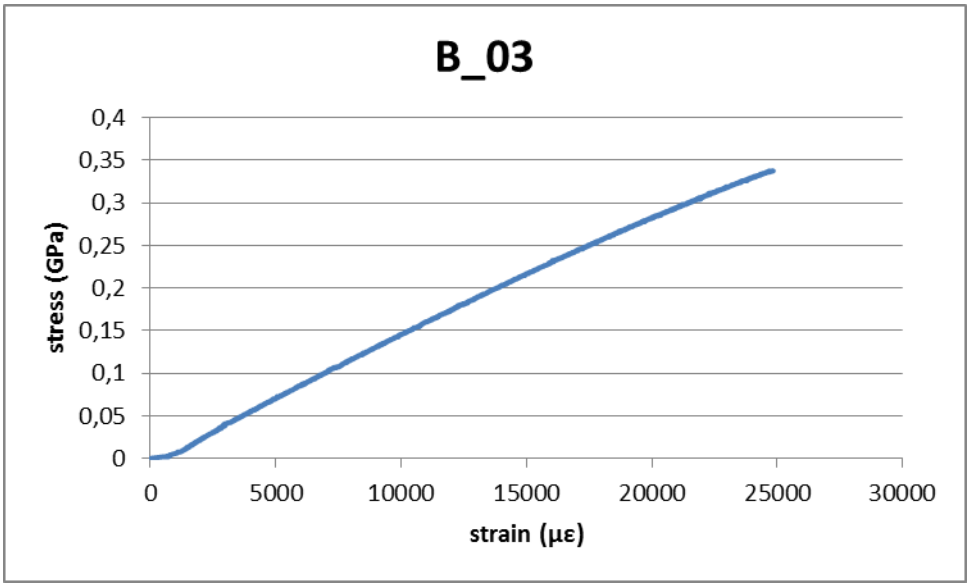

Figure A.9: Stress-strain diagram for specimen 3 of case “B” (Epoxy HLU-post cured).

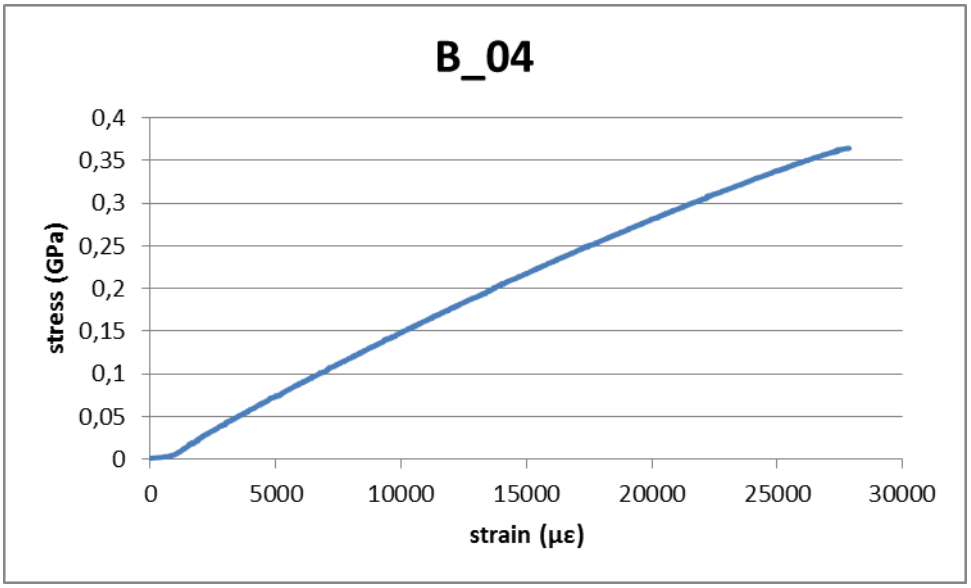

Figure A.10: Stress-strain diagram for specimen 4 of case “B” (Epoxy HLU-post cured).

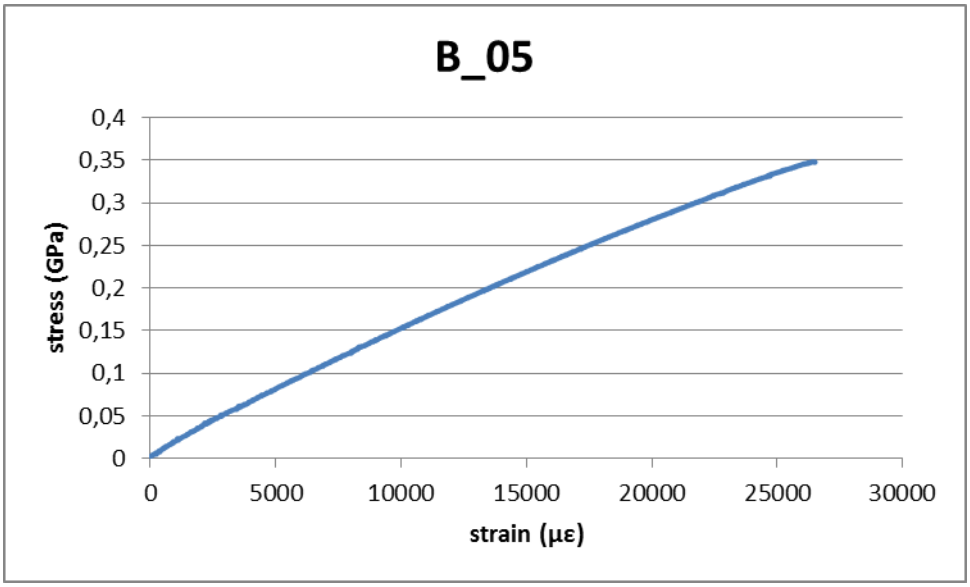

Figure A.11: Stress-strain diagram for specimen 5 of case “B” (Epoxy HLU-post cured).

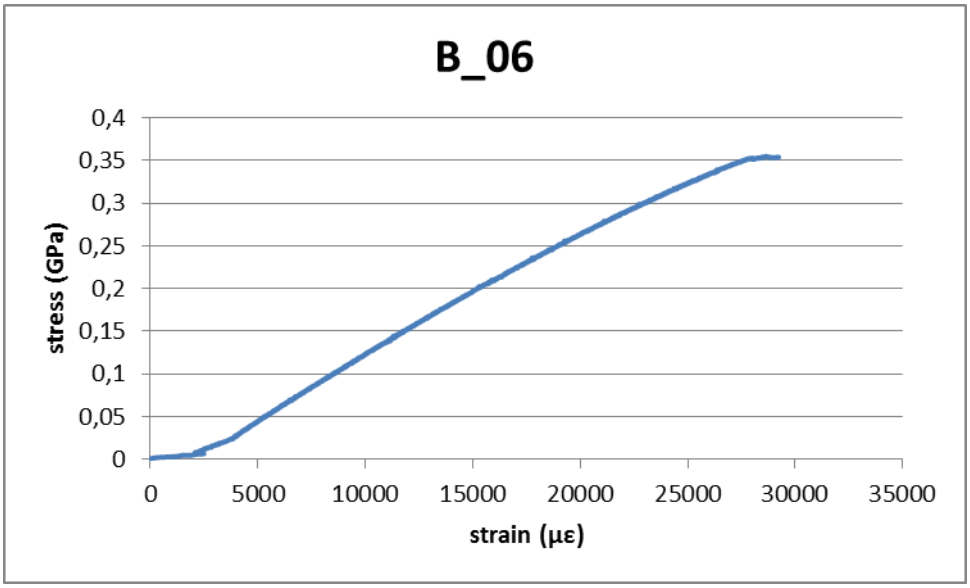

Figure A.12: Stress-strain diagram for specimen 6 of case “B” (Epoxy HLU-post cured).

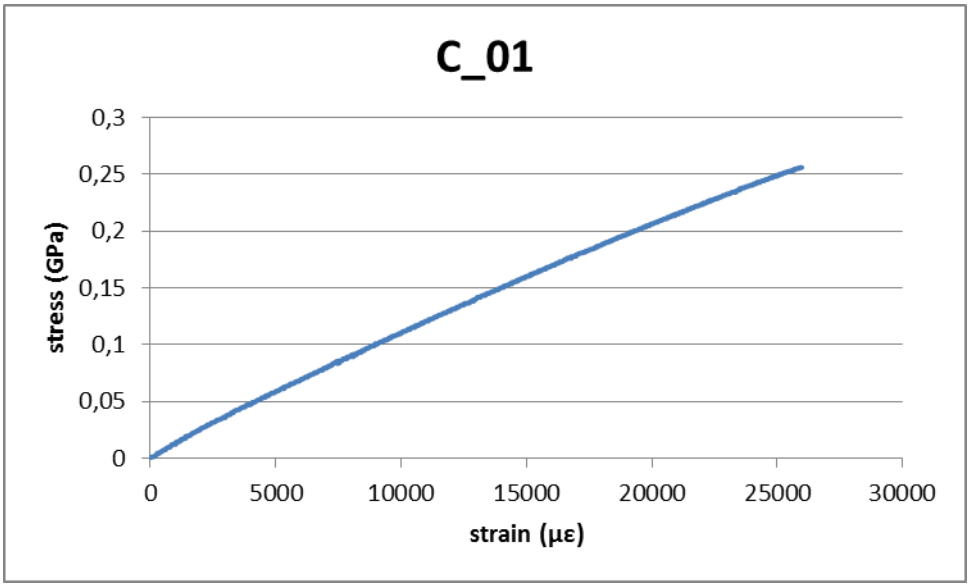

Figure A.13: Stress-strain diagram for specimen 1 of case “C” (Epoxy, vacuum bagging-cold cured).

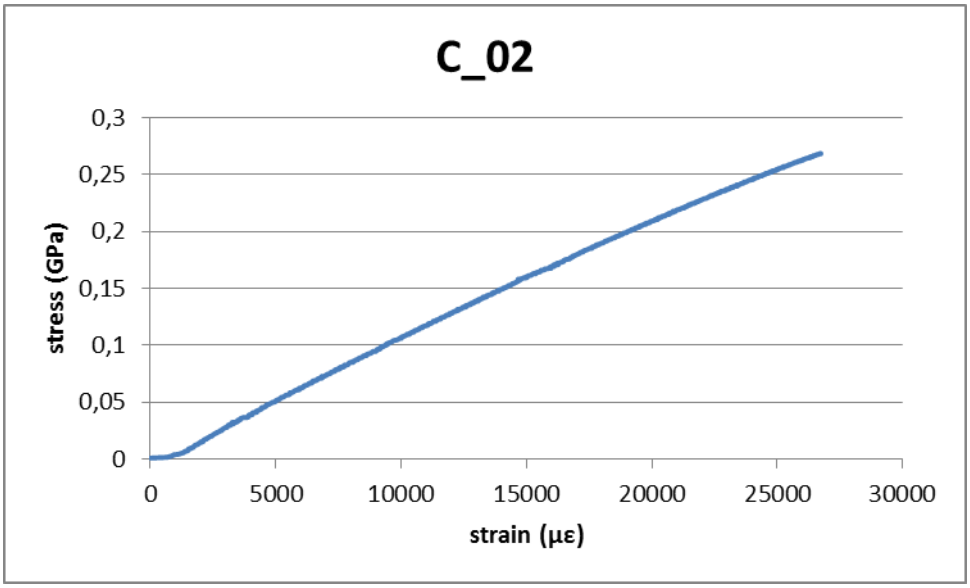

Figure A.14: Stress-strain diagram for specimen 2 of case “C” (Epoxy, vacuum bagging-cold cured).

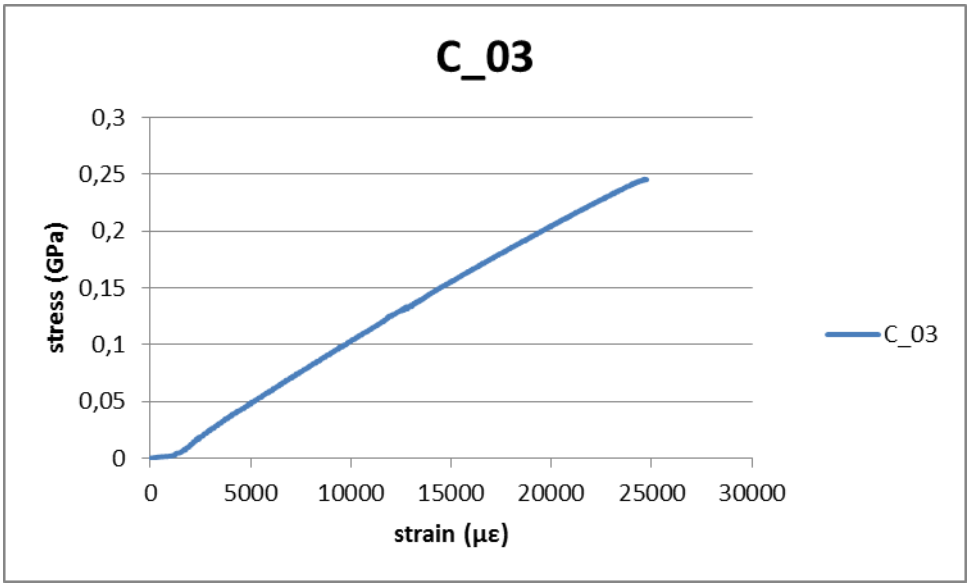

Figure A.15: Stress-strain diagram for specimen 3 of case “C” (Epoxy, vacuum bagging-cold cured).

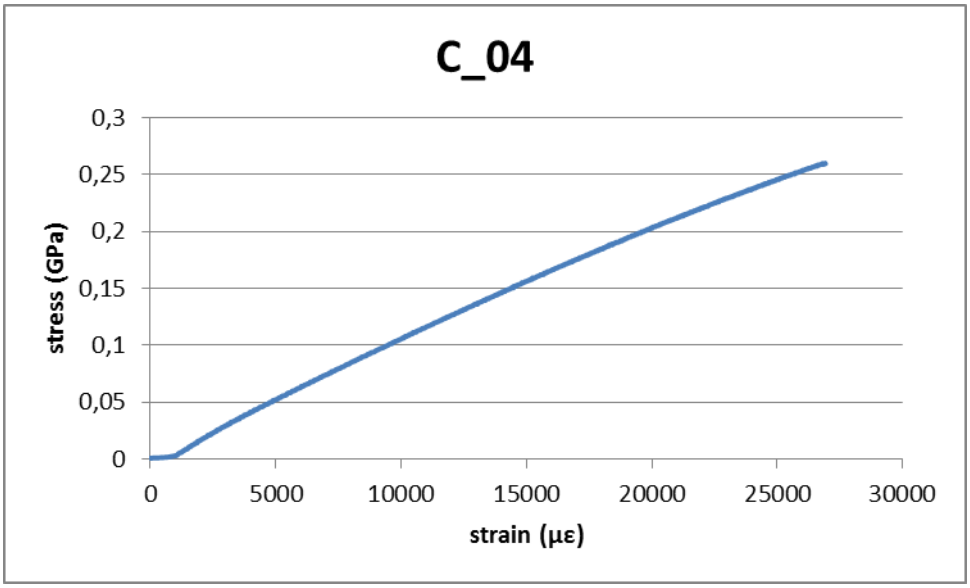

Figure A.16: Stress-strain diagram for specimen 4 of case “C” (Epoxy, vacuum bagging-cold cured).

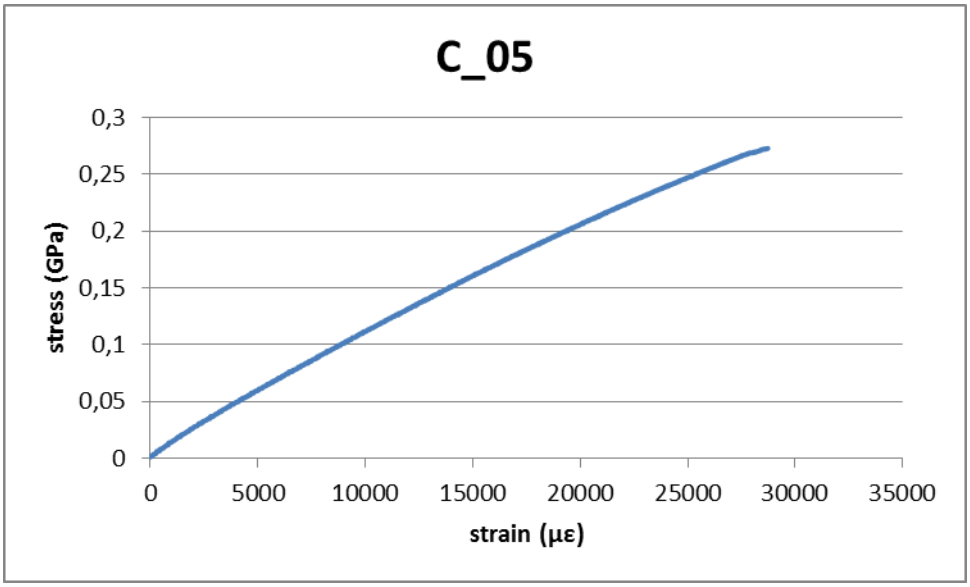

Figure A.17: Stress-strain diagram for specimen 5 of case “C” (Epoxy, vacuum bagging-cold cured).

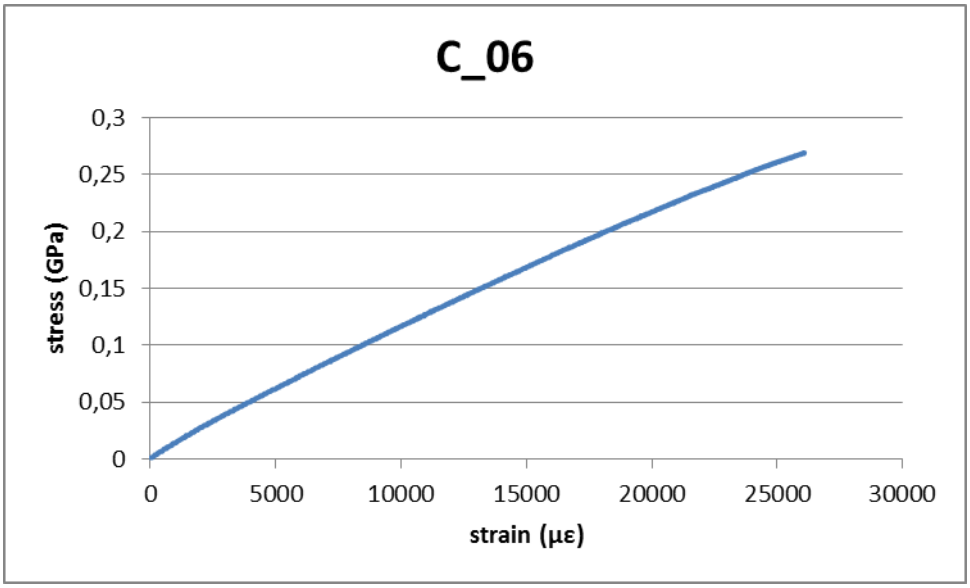

Figure A.18: Stress-strain diagram for specimen 6 of case “C” (Epoxy, vacuum bagging-cold cured).

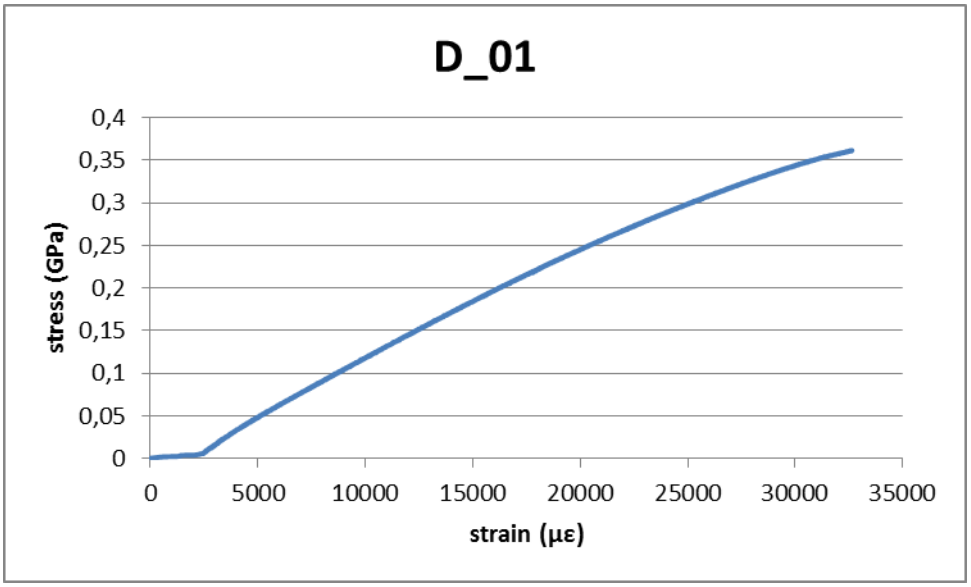

Figure A.19: Stress-strain diagram for specimen 1 of case “D” (Epoxy, vacuum bagging-post cured).

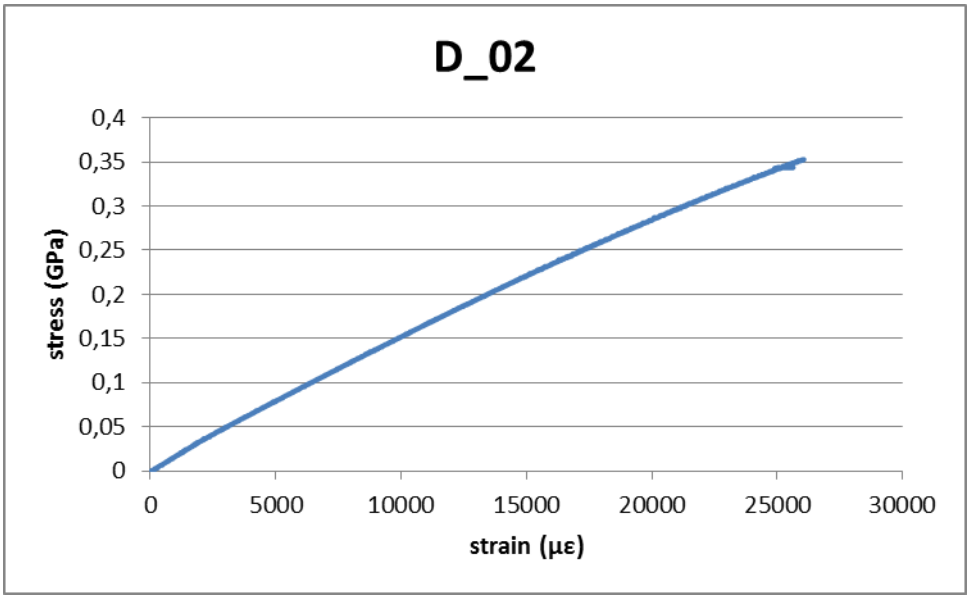

Figure A.20: Stress-strain diagram for specimen 2 of case “D” (Epoxy, vacuum bagging-post cured).

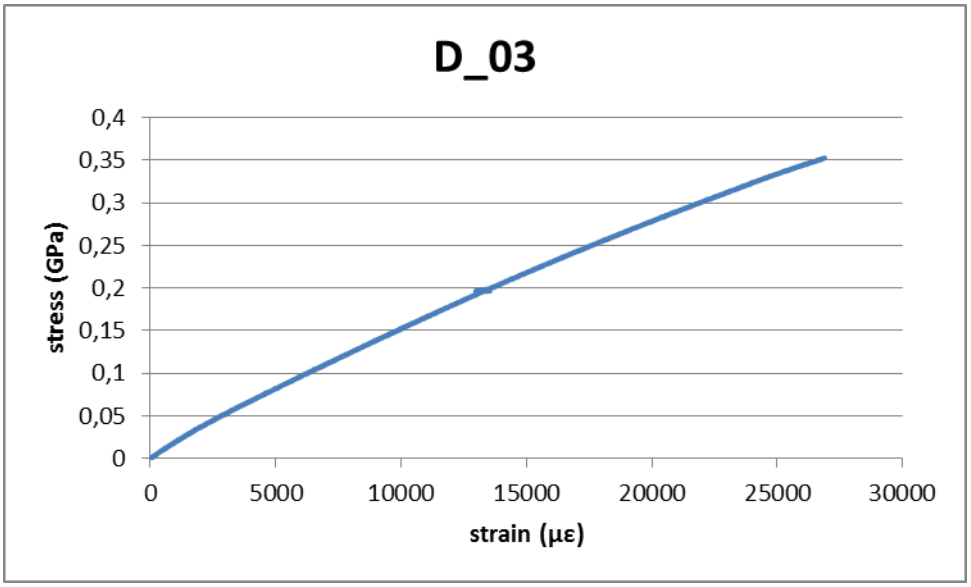

Figure A.21: Stress-strain diagram for specimen 3 of case “D” (Epoxy, vacuum bagging-post cured).

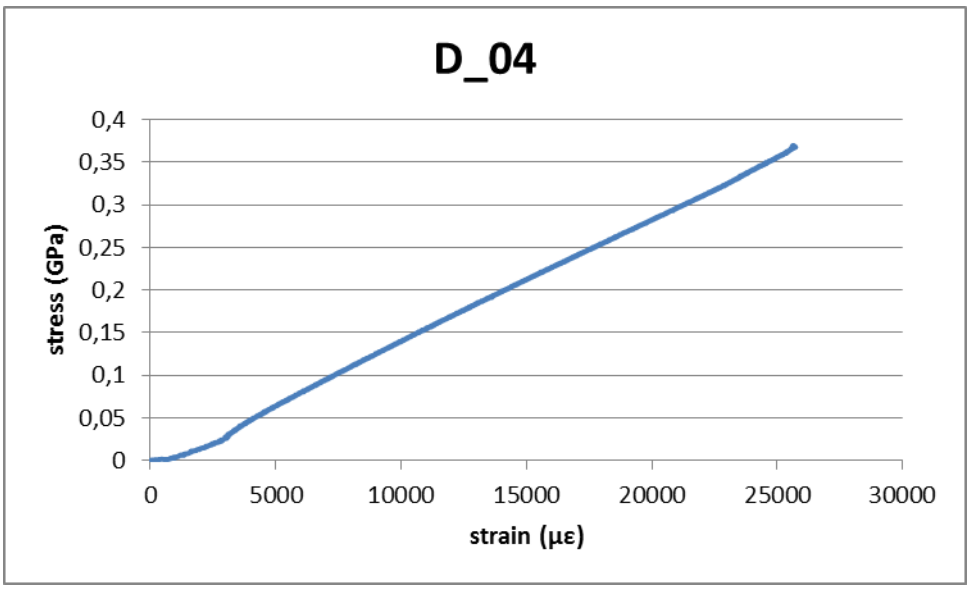

Figure A.22: Stress-strain diagram for specimen 4 of case “D” (Epoxy, vacuum bagging-post cured).

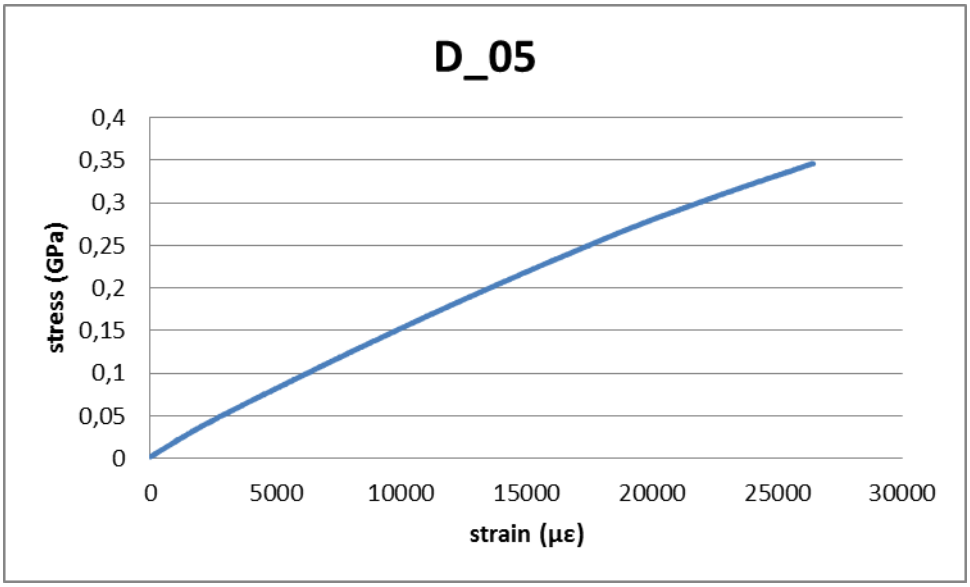

Figure A.23: Stress-strain diagram for specimen 5 of case “D” (Epoxy, vacuum bagging-post cured).

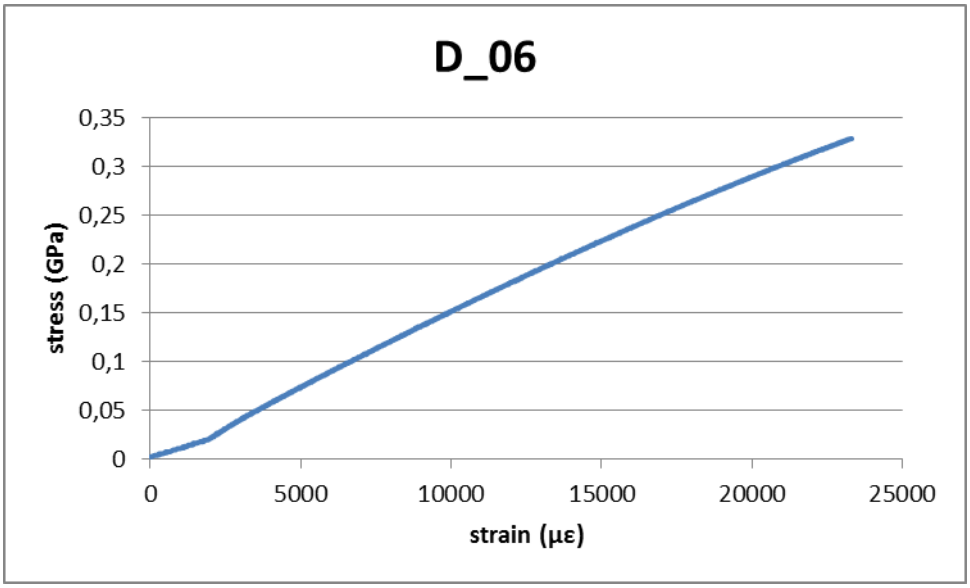

Figure A.24: Stress-strain diagram for specimen 6 of case “D” (Epoxy, vacuum bagging-post cured).

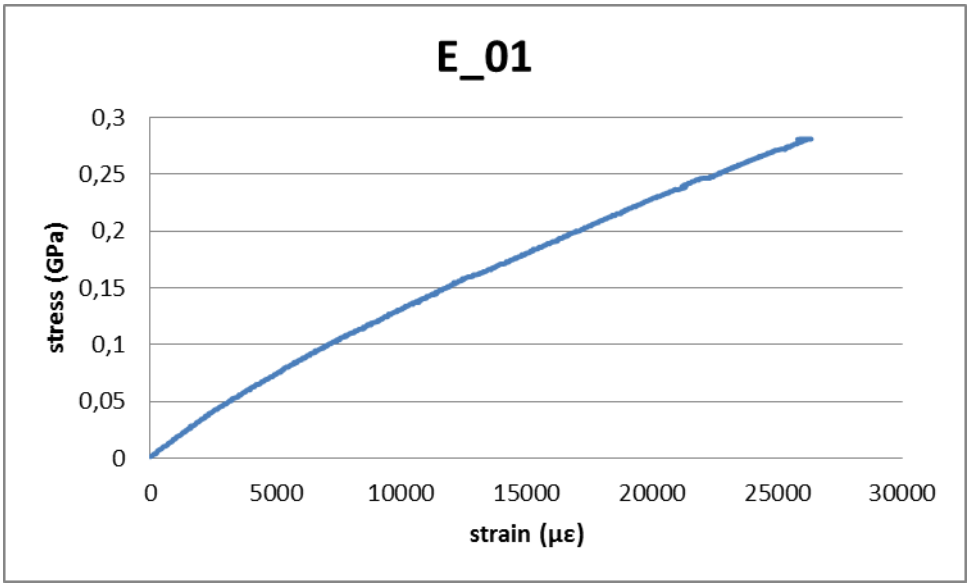

Figure A.25: Stress-strain diagram for specimen 1 of case “E” (Polyester HLU, cold cured).

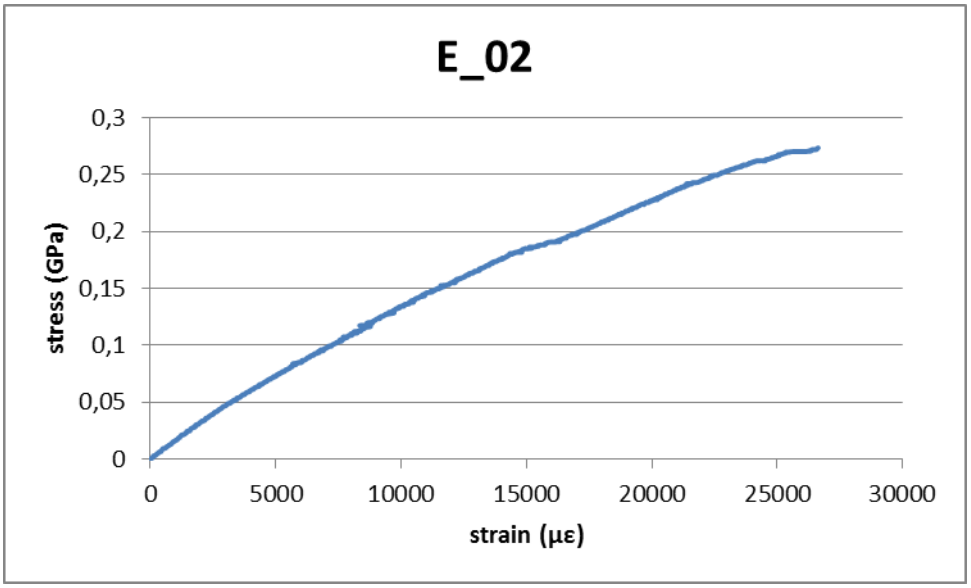

Figure A.26: Stress-strain diagram for specimen 2 of case “E” (Polyester HLU, cold cured).

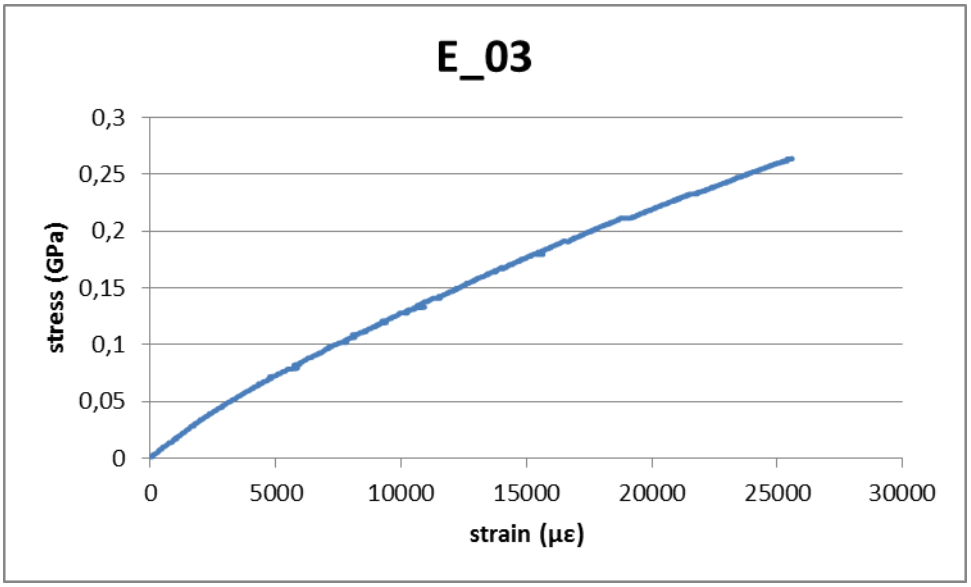

Figure A.27: Stress-strain diagram for specimen 3 of case “E” (Polyester HLU, cold cured).

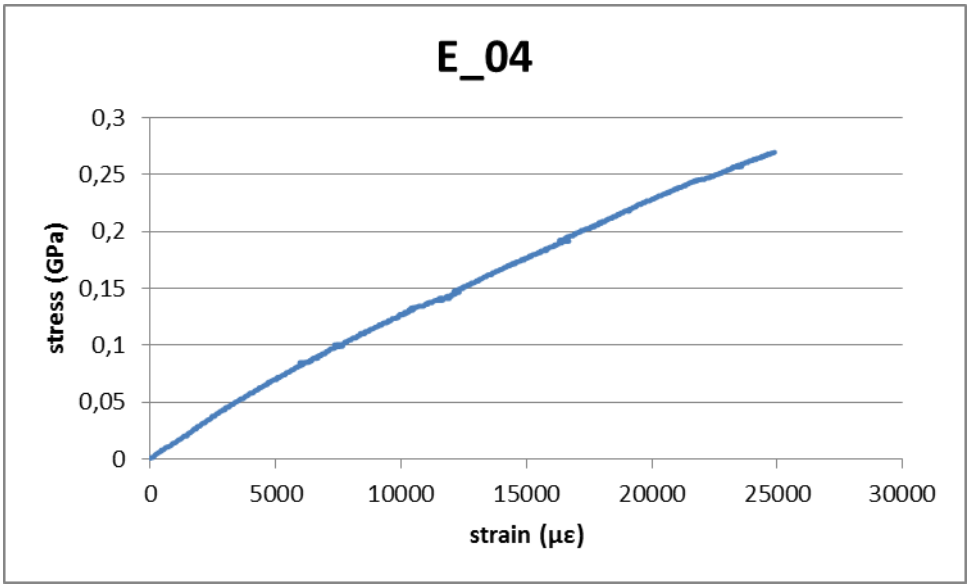

Figure A.28: Stress-strain diagram for specimen 4 of case “E” (Polyester HLU, cold cured).

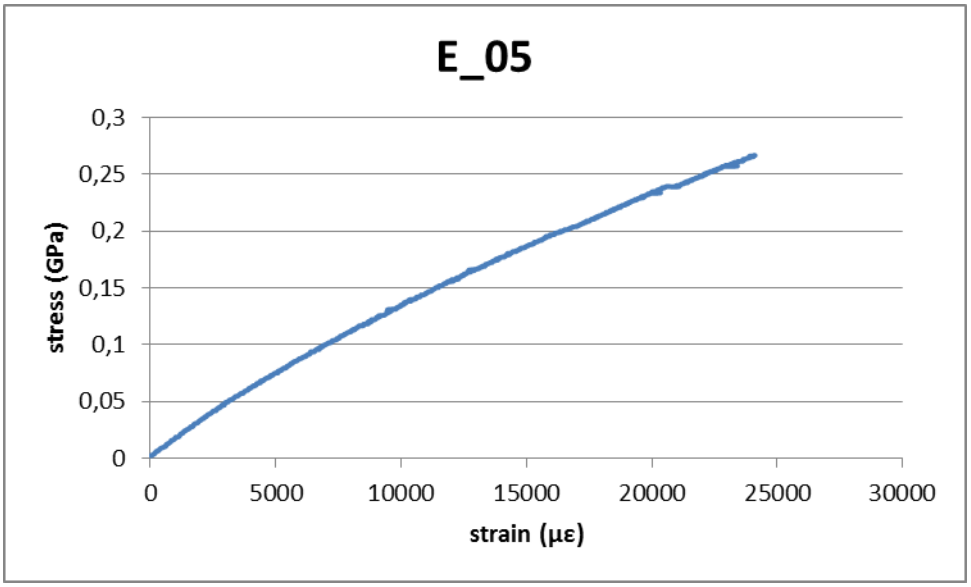

Figure A.29: Stress-strain diagram for specimen 5 of case “E” (Polyester HLU, cold cured).

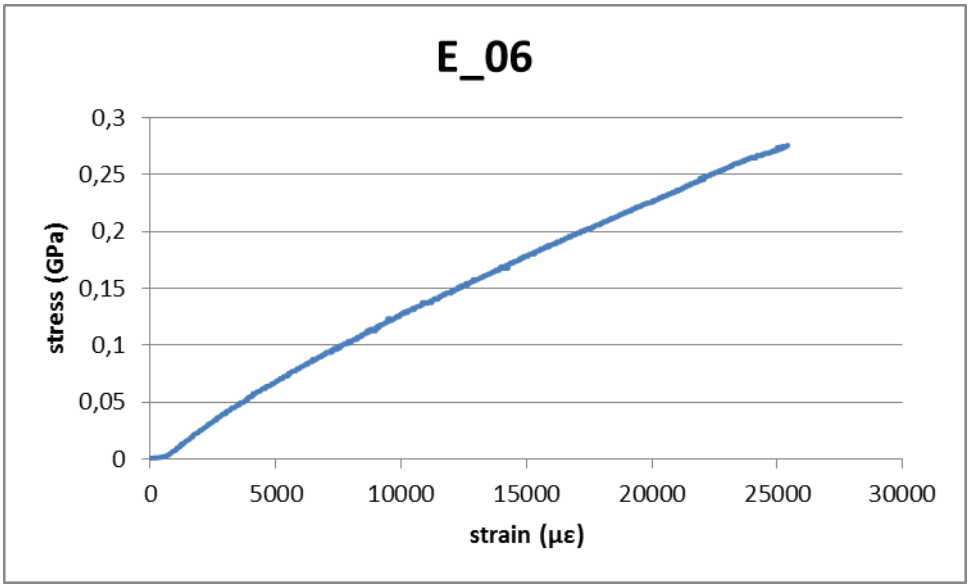

Figure A.30: Stress-strain diagram for specimen 6 of case “E” (Polyester HLU, cold cured).